Intermittent Ca^{2+} signals mediated by Orai1 regulate basal T cell motility

Tobias X. Dong[1,2], Shivashankar Othy[1,2], Milton L. Greenberg[1], Amit Jairaman[1], Chijioke Akunwafo[1], Sabrina Leverrier[1], Ying Yu[1], Ian Parker[1,3], Joseph L. Dynes[1], and Michael D. Cahalan[1,4]

[1]Department of Physiology and Biophysics, University of California, 285 Irvine Hall, Irvine, California 92697, USA.

[2]Co-first authors

[3]Department of Neurobiology & Behavior, University of California, McGaugh Hall, Irvine, California 92697, USA.

[3]Institute for Immunology, University of California, 285 Irvine Hall, Irvine, California 92697, USA.

*Corresponding Author: Michael D. Cahalan (mcahalan@uci.edu)

Key Words: T cell motility, Orai1, genetically encoded Ca^{2+} indicator, Ca^{2+} signaling, two-photon microscopy

Abstract

Ca^{2+} influx through Orai1 channels is crucial for several T cell functions, but a role in regulating basal cellular motility has not been described. Here we show that inhibition of Orai1 channel activity increases average cell velocities by reducing the frequency of pauses in human T cells migrating through confined spaces, even in the absence of extrinsic cell contacts or antigen recognition. Utilizing a novel ratiometric genetically encoded cytosolic Ca^{2+} indicator, Salsa6f, which permits real-time monitoring of cytosolic Ca^{2+} along with cell motility, we show that spontaneous pauses during T cell motility in vitro and in vivo coincide with episodes of cytosolic Ca^{2+} signaling. Furthermore, lymph node T cells exhibited two types of spontaneous Ca^{2+} transients: short-duration “sparkles” and longer duration global signals. Our results demonstrate that spontaneous and self-peptide MHC-dependent activation of Orai1 ensures random walk behavior in T cells to optimize immune surveillance.

To initiate the adaptive immune response, T cells must make direct contact with antigen-presenting cells (APCs) in the lymph node, enabling T cell receptors (TCRs) to engage peptide-bound MHC molecules presented on the APC surface. Because cognate antigens are rare for any given TCR, many APCs must be scanned to identify those bearing cognate antigens. Thus, optimizing T cell motility to balance search sensitivity, specificity, and speed is crucial for efficient antigen search and proper immune function (Cahalan and Parker 2005, Krummel, Bartumeus et al. 2016). Both cell-intrinsic and environmental factors have been proposed to regulate T cell motility within lymph nodes and peripheral tissues (Miller, Wei et al. 2002, Bousso and Robey 2003, Mempel, Henrickson et al. 2004, Mrass, Petravic et al. 2010). T cell motility in steady-state lymph nodes under homeostatic conditions, referred to as “basal motility”, has been likened to diffusive Brownian motion, resembling a “stop-and-go” random walk that results in an overall exploratory spread characterized by a linear mean-squared displacement over time (Miller, Wei et al. 2002). Subsequent studies defined a role of cellular cues in guiding T cell migration, such as contact with the lymph node stromal cell network or short-term encounters with resident dendritic cells (Miller, Hejazi et al. 2004, Bajenoff, Egen et al. 2006, Khan, Headley et al. 2011). Whereas the basic signaling mechanisms for cell-intrinsic induction of random motility have been previously explored in fibroblasts and neuroblastoma cells (Petrie, Doyle et al. 2009), it remains unclear if such mechanisms apply in T cells.

Upon T cell recognition of cognate antigen, TCR engagement results in an elevated cytosolic Ca^{2+} concentration that acts as a “STOP” signal to halt motility and anchor the T cell to the site of antigen presentation (Donnadieu, Bismuth et al. 1994,

Negulescu, Krasieva et al. 1996, Dustin, Bromley et al. 1997, Bhakta, Oh et al. 2005, Moreau, Lemaitre et al. 2015). The predominant mechanism for increasing cytosolic Ca^{2+} in T cells is through store-operated Ca^{2+} entry (SOCE), which is mediated by the molecular components STIM1 and Orai1. TCR stimulation triggers depletion of intracellular Ca^{2+} stores in the endoplasmic reticulum (ER), resulting in translocation of the ER-resident Ca^{2+} sensor STIM1 to specialized ER-plasma membrane (PM) junctions where Orai1 channels aggregate into puncta and activate to allow sustained Ca^{2+} influx (Liou, Kim et al. 2005, Roos, DiGregorio et al. 2005, Zhang, Yu et al. 2005, Luik, Wu et al. 2006, Vig, Beck et al. 2006, Zhang, Yeromin et al. 2006, Calloway, Vig et al. 2009, Wu, Covington et al. 2014). Orai1 channel activity is crucial for immune function, as human mutations in Orai1 result in severe combined immunodeficiency (SCID) (Feske, Gwack et al. 2006). Additional roles of Orai1 have been defined in chemotaxis to certain chemokines and T cell homing to lymph nodes (Greenberg, Yu et al. 2013); actin cytoskeleton rearrangement (Schaff, Dixit et al. 2010, Dixit, Yamayoshi et al. 2011, Babich and Burkhardt 2013, Hartzell, Jankowska et al. 2016); migration during shear flow (Schaff, Dixit et al. 2010, Dixit, Yamayoshi et al. 2011); lipid metabolism (Maus, Cuk et al. 2017); and dendritic spine maturation in neurons (Korkotian, Oni-Biton et al. 2017). However, despite their contributions to other aspects of T cell function, no role has been identified for Orai1 channels in T cell motility patterns underlying scanning behavior.

In this study, we use human and mouse T cells to assess the role of Orai1 and Ca^{2+} ions in regulating basal cell motility. Expression of a dominant-negative Orai1-E106A construct was used to block Orai1 channel activity in human T cells, both in vivo within immunodeficient mouse lymph nodes (Greenberg, Yu et al. 2013), and in vitro within

microfabricated polydimethylsiloxane (PDMS) chambers (Jacobelli, Friedman et al. 2010). We use our genetically encoded Salsa6f tandem green/red fluorescent Ca^{2+} indicator (**eLIFE submission # 29-09-2017-ISRA-eLife-32417)** to monitor spontaneous Ca^{2+} signaling in human T cells migrating in confined microchannels in vitro. Finally, using a transgenic mouse strain expressing Salsa6f in $CD4^+$ T cells, designated as CD4-Salsa6f$^{+/+}$ mice from here on, we show that Ca^{2+} signals occur in the absence of specific antigen as T cells crawl in the lymph node. Our results indicate that Ca^{2+} influx, activated intermittently through Orai1 channels, triggers spontaneous pauses during T cell motility and fine-tunes the random-walk search for cognate antigens.

Results

Inhibition of Orai1 in human T cells using a dominant-negative construct

To study the role of Orai1 channel activity in T cell motility, we transfected human T cells with the dominant-negative mutant Orai1-E106A to selectively eliminate ion conduction through the Orai1 pore. The glutamate residue at position 106 in human Orai1 forms the selectivity filter of the Orai1 pore (Prakriya, Feske et al. 2006, Vig, Beck et al. 2006, Yeromin, Zhang et al. 2006), and because the Orai1 channel is a functional hexamer (Hou, Pedi et al. 2012), mutation of E106 to neutrally charged alanine completely inhibits Ca^{2+} permeation in a potent dominant-negative manner (Greenberg, Yu et al. 2013). Using Fura-2 based Ca^{2+} imaging, we confirmed Orai1 channel block by E106A in activated human T cells transfected with either eGFP-tagged Orai1-E106A or empty vector for control. Thapsigargin induced SOCE was greatly diminished in cells expressing eGFP-Orai1-E106A, referred to here as eGFP-E106^{hi} T cells, compared to empty vector-transfected control cells (**Figure 1A**). Ca^{2+} entry was also partially inhibited in a population of transfected T cells with minimal eGFP fluorescence referred to as eGFP-E106A^{lo} cells. To confirm that eGFP-E106A inhibits T cell activation, we challenged transfected human T cells with autologous dendritic cells pulsed with the superantigen Staphylococcal enterotoxin B (Lioudyno, Kozak et al. 2008). T cell proliferation was markedly suppressed in eGFP-E106A^{hi} CD4^{+} and CD8^{+} T cells, but not in eGFP-E106A^{lo} T cells (**Figure 1B**). This shows that the residual Orai1 channel activity in eGFP-E106A^{lo} T cells is sufficient for T cell activation and proliferation. Taken together, these experiments show that eGFP-tagged Orai1-E106A expression can serve as a robust tool to assess cellular roles of

Orai1 channel activity, and that transfected cells without detectable eGFP fluorescence can be used as an internal control.

Orai1 function in human T cell motility was evaluated in vivo using a human xenograft model in which immunodeficient NOD.SCID.β2 mice were reconstituted with human peripheral blood lymphocytes, followed by imaging of excised lymph nodes using two-photon microscopy (Greenberg, Yu et al. 2013). Reconstitution has been shown to produce a high density of human immune cells within the lymph nodes of immunodeficient mice (Mosier, Gulizia et al. 1988), simulating the crowded migratory environment experienced by T cells under normal physiological conditions. Three weeks after reconstitution, human T cells were purified from the same donor, transfected, and adoptively transferred into the reconstituted NOD.SCID.β2 mice (**Figure 1-figure supplement 1**). Whereas control T cells transfected with eGFP showed robust expression and successfully homed to lymph nodes following adoptive transfer 24 hr post-transfection, eGFP-E106A transfected T cells did not home to lymph nodes in the same period, consistent with our previous study indicating that functional Orai1 channel activity is required for T cell homing to lymph nodes (Greenberg, Yu et al. 2013). To circumvent the homing defect, we injected eGFP-E106A transfected T cells only 3 hr post-transfection, before the expression level of eGFP-E106A had become sufficiently high to block lymph node entry (**Figure 1C**).

Orai1 block increases human T cell motility within intact lymph node

To evaluate Orai1 function in T cell motility, we imaged human T cells within intact lymph nodes of reconstituted NOD.SCID.β2 mice by two-photon microscopy (**Figure 2A**). We

found that eGFP-E106A^{hi} T cells migrated with significantly higher average velocities than co-transferred, mock-transfected CMTMR-labeled T cells (**Figure 2B**). Although both populations had similar maximum and minimum instantaneous cell velocities (**Figure 2C**), eGFP-E106A^{hi} T cells traversed longer distances compared to CMTMR controls (**Figure 2D**), and directionality ratios, a measure of track straightness, decayed more slowly (**Figure 2E**) indicating straighter paths when Orai1 channels were blocked. Orai1-blocked cells displayed shallower turn angles than controls (**Figure 2F**). Furthermore, arrest coefficients, defined by the fraction of time that cell velocity was < 2 μm/min, was six-fold lower for eGFP-E106A^{hi} T cells than for control T cells (**Figure 2G**). These differences in motility suggest that the increase in average cell velocity caused by Orai1 block is not due to eGFP-E106A^{hi} T cells moving faster than control T cells, but rather due to a reduced frequency of pausing. Consistent with this interpretation, no eGFP-E106A^{hi} T cells with average velocities < 7 μm/min were observed, unlike control T cells in which 23% of average velocities were < 7 μm/min (**Figure 2H**).

To replicate our findings in a different immunodeficient mouse model, we repeated our human T cell adoptive transfer protocol using NOD.SCID mice depleted of NK cells. Lymph nodes in these mice are small and contain reticular structures but are completely devoid of lymphocytes (Shultz, Schweitzer et al. 1995). Similar to experiments on reconstituted NOD.SCID.β2 mice, eGFP-E106A^{hi} human T cells in NOD.SCID lymph nodes migrated with significantly elevated average velocities compared to control T cells (**Figure 2I**), and exhibited lower arrest coefficients (**Figure 2J**). Both eGFP-E106A^{hi} and control T cells migrated at lower speeds in the NK-depleted NOD.SCID model compared to the reconstituted NOD.SCID.β2 model. Because control human T cells in reconstituted

NOD.SCID.β2 lymph nodes migrated at similar speeds to wildtype mouse T cells in vivo (Miller, Wei et al. 2002), reconstitution results in a lymph node environment that more closely mimics normal physiological conditions. Furthermore, the greater effect of Orai1 block on T cell arrest coefficients in crowded reconstituted lymph nodes suggests that Orai1's role in motility is more pronounced in crowded cell environments.

Orai1 channel activity triggers pauses during human T cell motility in vitro in the absence of extrinsic cell contact

To evaluate whether the pronounced effect of Orai1 channel block on the arrest coefficient in reconstituted lymph nodes was a result of environmental factors such as increased cellular contacts or increased confinement, we tracked human T cells in microfabricated PDMS chambers with cell-sized microchannels 7 μm high x 8 μm wide. These ICAM-1 coated microchannels simulate the confined environment of densely packed lymph nodes (Jacobelli, Friedman et al. 2010), while eliminating possible cell-extrinsic factors. Transfected human T cells were activated with plate-bound anti-CD3/28 antibodies and soluble IL-2, then dropped into chambers and monitored by time-lapse confocal microscopy, using phase contrast to visualize eGFP-E106A^{lo} T cells (**Figure 3A,B**). Upon entry into microchannels, eGFP-E106A^{hi} T cells migrated with higher average cell velocities than eGFP-E106A^{lo} T cells (**Figure 3C**), similar to our in vivo findings from intact lymph node (*c.f.*, **Figures 3C, 6B**). To ensure that the observed difference in cell velocity was due to suppressed Orai1 channel function and not overexpression of Orai1 protein, we also tracked T cells transfected with eGFP-tagged wildtype Orai1. Both eGFP-Orai1^{hi} and eGFP-Orai1^{lo} T cells migrated at the same

average cell velocity (**Figure 3C**), demonstrating that Orai1 channel overexpression, in itself, does not perturb T cell motility in microchannels. Since eGFP-E106A^{lo} T cells have reduced Orai1 channel activity but still retain the same cell velocity as eGFP-Orai1 transfected T cells (*c.f.*, **Figures 1A, 3C**), this suggests that partial Orai1 function is sufficient to generate normal pausing frequency in confined environments. The frequency distribution of cell velocities in vitro is comparable to our in vivo data: fewer GFP-E106A^{hi} T cells migrated with average cell velocities < 7 μm/min as compared to eGFP-E106A^{lo} T cells (11% vs 29%; *c.f.*, **Figures 3D, 2G**). Furthermore, eGFP-E106A^{hi} T cells exhibited lower arrest coefficients (**Figure 3E**) and less variation in velocity than eGFP-E106A^{lo} T cells (**Figure 3F**). Although eGFP-E106A^{hi} T cells had lower arrest coefficients, the durations of their pauses were not significantly different than in eGFP-E106A^{lo} T cells (**Figure 3G**). Taken together, the reduced arrest coefficients in eGFP-E106A^{hi} T cells indicate that inhibition of Orai1 channel activity results in reduced frequency of pauses during T cell motility. These in vitro results confirm our in vivo findings and support the hypothesis that Orai1 activity intermittently triggers cell arrest, resulting in an overall decrease in motility within confined environments. Moreover, since our in vitro microchannel assay eliminates extrinsic cell-cell interactions, this indicates that Orai1 can be spontaneously activated to modulate T cell motility.

Spontaneous Ca^{2+} signals during confined motility in vitro are correlated with reduced T cell velocity

To study the correlation between Ca^{2+} signals and T cell motility, human $CD4^+$ T cells were transfected with Salsa6f, a novel genetically encoded Ca^{2+} indicator consisting of

tdTomato fused to GCaMP6f, activated the T cells for two days with plate-bound anti-CD3/28 antibodies, then dropped into ICAM-1 coated microchambers. As previously shown (**eLIFE submission # 29-09-2017-ISRA-eLife-32417**), Salsa6f is localized to the cytosol, with red fluorescence from tdTomato that reflects fluctuations in cell movement and very low baseline green fluorescence from GCaMP6f that rises sharply during Ca^{2+} signals (**Figure 4A-D**). Salsa6f-transfected human T cells were tracked in both confined microchannels (**Figure 4A**, **Video 1**) and the open space adjacent to entry into microchannels (**Figure 4C**, **Video 2**), to evaluate T cell motility under varying degrees of confinement. Intracellular Ca^{2+} levels were monitored simultaneously using the ratio of total GCaMP6f fluorescence intensity over total tdTomato fluorescence intensity (designated as G/R ratio), enabling detection of a notably stable baseline ratio unaffected by motility artifacts in moving T cells while reporting spontaneous Ca^{2+} signals that could be compared to changes in motility (**Figure 4B,D**, orange and black traces, respectively).

Human T cells expressing Salsa6f migrating in confined microchannels exhibited sporadic Ca^{2+} signals as brief peaks unrelated to changes in cell velocity, or as more sustained periods of Ca^{2+} elevation associated with reduced cell velocity (**Figure 5A,B**). To evaluate the correlation between T cell velocity and Ca^{2+} signals, we compared average T cell velocities during periods of sustained Ca^{2+} elevations to average velocities at baseline Ca^{2+} levels. T cell velocity decreased significantly when cytosolic Ca^{2+} was elevated above baseline (5.9 ± 0.1 μm/min vs. 10.0 ± 0.1 μm/min, $p < 0.0001$; **Figure 5C**). Ca^{2+} signaling episodes that last for 30 seconds or longer accompany and appear to closely track the duration of pauses in cell movement. Comparison of instantaneous velocities with corresponding cytosolic Ca^{2+} signals (G/R ratio) by scatter plot revealed a

strong inverse relationship: highly motile T cells always exhibited baseline Ca^{2+} levels, while elevated Ca^{2+} levels were only found in slower or arrested T cells (**Figure 5D**). It is important to note that these Ca^{2+} signals and reductions in velocity occurred in the absence of any extrinsic cell contact or antigen recognition, indicating that Ca^{2+} elevations, like pausing and Orai1 activation, can be triggered in a cell-intrinsic manner.

To compare the effects of Orai1 activity on the motility of T cells in a less confined environment, we also monitored T cell migration within the open space in PDMS chambers adjacent to entry into microchannels (*c.f.*, **Figure 4A,C**). We reasoned that in this two-dimensional space with reduced confinement, T cells may not gain sufficient traction for rapid motility, and instead may favor integrin-dependent sliding due to increased exposure to the ICAM-1 coated surface (Krummel, Friedman et al. 2014). In addition, the same population of T cells could be tracked as they migrated into and along the confined microchannels, providing a valuable internal control. We found that eGFP-E106A^{hi} T cells migrated with similar velocities to eGFP-E106A^{lo} T cells in the open space, but these eGFP-E106A^{hi} T cells still exhibited higher motility in the microchannels than eGFP-E106A^{lo} T cells (**Figure 5E**). Furthermore, Salsa6f-transfected T cells within the open space rarely produced Ca^{2+} transients (*c.f.*, **Figure 5D,F**, top left quadrants, 13% of the time in microchannels vs 2% in open space), implying that Ca^{2+} elevations, and by extension, Orai1 channel activity, do not generate pauses when T cells are reliant on integrin binding for motility. Consistent with this, differentiated Th1 cells from CD4-Salsa6f mice also showed similar instantaneous velocities and only rare Ca^{2+} transients when plated on open-field ICAM-coated coverslips (**Figure 5-figure supplement 1**). Taken

248 together, these experiments establish a role for Orai1 channels and Ca^{2+} influx in
249 modulating T cell motility within confined environments.
250
251 **Spontaneous T cell Ca^{2+} transients during basal motility in the lymph node**
252 Using Salsa6f, expressed in a CD4-Cre dependent transgenic model we have reported
253 that mouse T cells exhibit frequent transient Ca^{2+} signals ("sparkles") in homeostatic
254 lymph nodes in the absence of specific antigen (**eLIFE submission # 29-09-2017-ISRA-**
255 **eLife-32417)**. To further analyze the relationship between Ca^{2+} signaling and motility in
256 detail within lymph nodes, we adoptively transferred CD4-Salsa6f$^{+/+}$ T cells into congenic
257 mice and, using two-photon microscopy in explanted recipient lymph nodes, tracked the
258 red tdTomato signal to establish cell position and the green CGaMP6f signal as a
259 measure of cytosolic Ca^{2+}. First, to delineate any adverse effect of Salsa6f on homing
260 and in situ motility of T lymphocytes, we co-injected equal numbers of CD4-Salsa6f$^{+/+}$ and
261 CD4-Cre control cells into WT recipients (**Figure 6A**). For simultaneous imaging and to
262 normalize any dye toxicity, CD4-Salsa6f$^{+/+}$ and CD4-Cre T cells were labeled with
263 CellTrace Yellow (CTY) and CellTrace Violet (CTV), respectively. Comparable numbers
264 of input cells were recovered from the subcutaneous lymph nodes after 18 hr (**Figure**
265 **6B**). Two-photon imaging and tracking in lymph nodes showed typical stop and go motility
266 and meandering cell tracks (**Figure 6C,D, Video 3**) for both cell types. Instantaneous 3D
267 velocities (**Figure 6E**) and mean track velocities (**Figure 6F**) were indistinguishable, as
268 was the decay rate of directionality ratio (**Figure 6H**). Furthermore, mean-squared
269 displacement (MSD) time analysis showed random-walk behavior for both cell types with

similar motility coefficients (**Figure 6H, I**). Altogether, motility characteristics of Salsa6f T cells are indistinguishable from control T cells.

To determine whether spontaneously occurring Ca^{2+} signals are correlated with motility, we transferred CD4-Salsa6f$^{+/+}$ cells alone into wildtype recipients and tracked red and green fluorescence intensities in the lymph nodes after 18 hr. Consistent with our previous observation, adoptively transferred T cells retained Salsa6f indicator in their cytosol, and Ca^{2+} signals were readily observed in motile Salsa6f^{+} T cells (**Figure 7A, Video 4**). We monitored the G/R ratios over time and observed a strong negative correlation between instantaneous cell velocity and Ca^{2+} levels (**Figure 7B)**. By examination of fluctuating cell velocity traces with corresponding G/R ratios, we found that the Ca^{2+} rise is clearly associated with a decrease in velocity (**Figure 7C and D**). Notably, on average, peaks of Ca^{2+} transients precede the average cell velocity minimum, suggesting that spontaneous rise in intracellular Ca^{2+} levels leads to cell pausing (**Figure 7E**).

Frequency, duration and MHC dependence of T cell Ca^{2+} transients in homeostatic lymph nodes.

Imaging adoptively transferred T cells in recipient lymph nodes is an ideal approach to probe in vivo T-cell motility. However, this approach is limiting when it comes to identifying the abundance and duration of Ca^{2+} signaling events, because transferred cells label only a fraction of the lymph node (< 1%) and longer imaging intervals are required to collect sufficient volume of 4D data (> 5 second). Therefore, to measure the endogenous frequency and duration Ca^{2+} transients, we imaged homeostatic CD4-Salsa6f$^{+/+}$ lymph

nodes at 2 frames per second. All endogenous T cells ($CD4^+$ and $CD8^+$) are labeled with the Salsa6f probe in CD4-Salsa6f$^{+/+}$ lymph nodes because T cells go through the double-positive stage during development in the thymus. More than 800 Ca^{2+} transients were identified in a 300 x 300 μm area in a 10-minute interval. We identified two types of Ca^{2+} transients: numerous small and brief spots (sparkles); and less frequent large, cell-wide transients (**Figure 8A, Video 5**). Consistent with our previous report (**eLIFE submission 29-09-2017-ISRA-eLife-32417**), most Ca^{2+} transients were localized to small regions of the cell and of short duration, spanning 2 μm^2 in area (**Figure 8B**) and lasting about 2 sec (**Figure 8C**). Altogether, the strong association of Ca^{2+} transients with reductions in cell velocity leading to pausing, and the sheer number of Ca^{2+} transients in homeostatic lymph nodes suggest that cytosolic Ca^{2+} is a key regulator of basal cellular motility under steady-state conditions in the absence of specific antigen.

Lymphocytes migrate in the immune dense micro-environment of secondary lymphoid tissues, constantly interacting with other immune cells, including resident antigen presenting cells (Germain, Robey et al. 2012)**.** Indeed, constant recognition of low levels of self-antigens through T cells receptor (TCR)-pMHC interactions is critical for maintaining sensitivity to foreign antigens (Stefanova, Dorfman et al. 2002); and deprivation (>7 days) of pMHC-II signals impairs T cell motility (Fischer, Jacovetty et al. 2007). To investigate whether Ca^{2+} signals in steady state lymph nodes are result of self-peptide recognition, we blocked MHC Class I and II signaling for 48 hr in CD4-Salsa6f$^{+/+}$ lymph nodes. The number of cell-wide events was not significantly different ($p = 0.06$), whereas the sparkle frequency was significantly decreased ($p = 0.02$) in MHC-blocked lymph nodes compared to isotype control (ITC) antibody treatment (**Figure 9A, D-G**).

There was also significant variation in the number of Ca^{2+} transients in ITC antibody and uninjected controls (Coefficient of variation = 41 to 45%), which may be due to the presence of heterogeneous antigen presenting cells displaying varying amount of self-peptides during steady-state. Most notably however, a significant number of Ca^{2+} transients remained even after MHC block, which we believe reflects a basal level of spontaneous Ca^{2+} activity independent of antigen recognition. In contrast, the intensity of individual Ca^{2+} transients in MHC blocked lymph nodes did not differ significantly from the ITC controls (**Figure 9B,C**). Altogether, our data indicate that T cells display substantial spontaneous Ca^{2+} transients even in absence of self-peptide recognition, suggesting a role in regulating basal T lymphocyte motility.

Discussion

In this study, we demonstrate that Orai1 channel activity regulates motility patterns that underlie immune surveillance. Human T cells expressing the dominant-negative Orai1-E106A construct migrated with higher average velocities than controls, both in reconstituted mouse lymph nodes in vivo and in confined microchannels in vitro. In particular, we found that the increase in average cell velocity was not due to an increase in maximum cell velocity, but to a reduced frequency of cell pausing accompanied by increased directional persistence, resulting in straighter paths. Human T cells demonstrate Ca^{2+} transient-associated and Orai1-dependent pauses in vitro within confined microchannels devoid of cell-extrinsic factors. Furthermore, we use a novel ratiometric genetically encoded Ca^{2+} indicator, Salsa6f, along with T cells from CD4-Salsa6f$^{+/+}$ transgenic mice, to show that intermittent Ca^{2+} signals coincide with reduced cell velocity. Treatment of CD4-Salsa6f$^{+/+}$ mice with MHC class-I and -II blocking antibodies substantially reduces but does not eliminate the frequent T cell Ca^{2+} transients seen in lymph nodes. Based on these findings, we propose that Orai1 channel activity regulates the timing of stop-and-go motility in T cells and tunes the search for cognate antigen in the crowded lymph node.

Our Orai1-E106A construct derives its specificity and potency by targeting the pore residue responsible for the channel selectivity filter. Incorporation of Orai1-E106A likely blocks heterodimers of Orai1 and other channels, such as Orai2 or Orai3, in addition to homomeric Orai1 channels. Very recent evidence demonstrates the existence of heteromeric channels composed of Orai1 and Orai2 in T cells (Vaeth, Yang et al. 2017). These heteromers appear to simply reduce the flow of Ca^{2+} through the Orai1 channel

without targeting additional signaling pathways. In the absence of contradictory evidence, we conclude that in T cells Orai1-E106A acts to produce an essentially complete functional knockdown of Orai1-mediated store-operated Ca^{2+} entry.

Human T cells exhibit systematic changes in motility behavior after Orai1 block, including: increased average velocity, fewer pauses, increased directional persistence and decreased turn angles, and increased motility spread over time. Importantly, maximum and minimum instantaneous velocities are unchanged. For human T cells assessed in motility assays in vitro, similar Orai1 dependent changes are seen. Altered pausing behavior caused by Orai1 block is displayed by isolated single cells inside microchannels formed from photolithographically precise silicon master molds. Changes in motility are dependent upon confinement, as Orai1 block alters pausing under confined but not open-field conditions. The absence of changes to maximum and minimum velocities in vivo and open field motility in vitro indicates that Orai1 block is not generally deleterious for cell health and movement, but instead acts upon subcellular mechanisms that are selectively employed during cell motility in confined spaces. Taken together, these systematic changes caused by Orai1 block reveal the presence of an Orai1-dependent cell motility program that is utilized frequently enough to be easily detected by changes in the motility characteristics of T cells in the lymph node.

We used CD4-Salsa6f$^{+/+}$ mice to track $CD4^+$ T cell Ca^{2+} signals in intact mouse lymph nodes and Salsa6f transient transfection to track Ca^{2+} signals in human T cells in vitro and in reconstituted mouse lymph nodes. In our companion paper, **eLIFE submission # 29-09-2017-ISRA-eLife-32417,** we show that Salsa6f expression in $CD4^+$ T cells is non-perturbing with respect to lymphocyte development, cellular phenotype, cell

proliferation, and differentiation. Here we demonstrate that homing to lymph nodes is unaffected, as are movement patterns within the lymph node, cell velocity, directional persistence, diffusive spread, and motility coefficient. We find that across cells, elevated Ca^{2+} levels are inversely correlated with instantaneous velocity, both in vitro and in vivo. In vivo, moving cells exhibit local Ca^{2+} signals that are strongly associated with pauses in motility. By inspection of movement patterns, turning is likely associated with Ca^{2+} signaling events as well, but this has not been established because most cells move outside of our shallow imaging field either before or after pausing. In many contexts, Ca^{2+} signaling has been shown not only to accompany, but also to cause cell arrest and loss of cell polarity, such as in T cells after activation by antigen (Negulescu, Krasieva et al. 1996, Dustin, Bromley et al. 1997, Wei, Safrina et al. 2007). By averaging events, the peak of subcellular Ca^{2+} transients was found to precede the velocity minimum. This event order is consistent with Ca^{2+} causing pauses. While we do not show that the Ca^{2+} signals we observe emanate directly from Orai1 channels, taken together our data are consistent with Orai1 actively regulating cell motility by directly inducing a subcellular motility program that leads to cell arrest.

Two-photon imaging indicated that the frequency of $CD4^+$ T cells Ca^{2+} transients varies widely between Salsa6f lymph nodes, even when events are normalized for different cell numbers. The origin of this variability is unclear, but may result from differences in the distribution and functional properties of APCs within the imaging field. Treatment of MHC class-I and –II blocking antibodies substantially reduces but does not eliminate T cells Ca^{2+} transients. Clearly, a significant number of Ca^{2+} transients are caused by T cell-APC interactions that act through MHC proteins. Given that Orai1 motility

events occur frequently as T cell migrate through the lymph node, and Ca^{2+} transients are associated with pauses in motility, we propose that spontaneously generated Orai1-dependent pauses and turns can be triggered by T cell-APC interaction through MHC proteins.

However, we find evidence for MHC-independent triggering of Ca^{2+} signaling and Orai1 channel activation in the lymph node. Human T cells exhibit Orai1-dependent pauses in vitro when migrating as isolated cells in highly uniform microchannels. Salsa6f expression independently detects Ca^{2+} transients in isolated T cells moving within microchannels but not in T cells in adjacent open field portions of the same PDMS imaging chamber. In both cases responses were produced in the absence of MHC proteins or APCs. Moreover, we note that, in paired experiments, treatment with MHC class-I and –II blocking antibodies leads to a reduced but notably consistent frequency of Ca^{2+} signaling events. Partial block would be expected to produce substantial variation, especially when combined with a variable input population. Taken together, these data point to the existence of not only MHC-independent Orai1 motility events, but also cell-intrinsic triggering of Orai1. Of note, the apparently random nature of naïve T cell movement in the lymph node has led to the hypothesis that T cells use intrinsic and stochastic motility mechanisms to accomplish immune surveillance (Wei, Parker et al. 2003, Mrass, Petravic et al. 2010, Germain, Robey et al. 2012).

In previous studies of Orai1 signaling, Orai1 activation has been placed downstream of extracellular ligand binding to cell surface receptors, integrating their input upon use-dependent depletion of Ca^{2+} from the ER (Feske 2007, Cahalan and Chandy 2009). While we expect signaling downstream of self-antigen detection to be the same as

for cognate antigens (Stefanova, Dorfman et al. 2002), at this point it is unclear which aspects of internal cell state might lead to cell-intrinsic opening of Orai1 channels and pauses in motility. Of particular interest is determining the step in the signaling cascade from phospholipase C to Orai1 that might be targeted by a novel cell-intrinsic activation pathway. Molecular candidates that underlie regulation of T cell motility by Ca^{2+} are less well defined. One clue to Orai1 action is the subcellular location of Ca^{2+} transients at the back T cells moving within intact lymph nodes, similar to the localization of Orai1 channels during movement in vitro (Barr, Bernot et al. 2008). Early studies demonstrated that immobilization and rounding of T cells bound to antigen presenting B cells occurred via a calcineurin-independent pathway (Negulescu, Krasieva et al. 1996). Ca^{2+} sensitive cytoskeletal proteins, such as myosin II or the actin bundling protein L-plastin, as good candidates for downstream effectors (Babich and Burkhardt 2013, Morley 2013). Like Orai1, Myosin 1g is selectively required for motility mechanisms under confined conditions (Gerard, Patino-Lopez et al. 2014). While Orai1 block reduces pausing but does not otherwise alter T cell velocity, Myo1g block increases pausing and causes cells to move faster. These differences in phenotype suggest that Orai1 and Myo1g act in different, and in part opposing, ways to control T cell motility.

Immune surveillance requires balancing many factors associated with antigen search, including speed and sensitivity (Friedl and Weigelin 2008, Krummel, Bartumeus et al. 2016). As moving T cells in the lymph node encounter APCs bearing antigen-MHC, they pause due to Ca^{2+} dependent mechanisms unleashed by Orai1 channel opening. These pauses likely ensure adequate time for TCR-antigen scanning by T cell-APC pairs. Our observations of T cell motility indicates that each T cell does not stop at every APC

441 it encounters. Because of this movement pattern, Orai1 provides attractive point of
442 regulation of immune surveillance. Increasing Orai1 activity might be expected to cause
443 T cells to pause more frequently when encountering APCs, restricting the distance T cells
444 move and offering increased opportunities for contact with nearby APCs. Alternatively,
445 decreasing Orai1 activity leads to fewer pauses, greater directional persistence, fewer
446 turns, and greater overall diffusive spread. In this way Orai1 channel activity could tailor
447 T cell excursions to match the density and reach of dendritic cells in the lymph node.
448 Finally, our findings provide further evidence that during resting conditions, TCR
449 interactions with self-MHC antigens drive continual but limited activation of downstream
450 signaling pathways.

451 We note some differences between our study and others involving Orai1, STIM1,
452 and T cell motility. These differences might be accounted for, in part, by the expected
453 consequences of our Orai1 dominant-negative approach: block of all three Orai isoforms,
454 limited time for compensatory changes in cell function, and restriction of Orai block to T
455 cells that are adoptively transferred after transfection. (1) Orai1/2 and STIM1/2 KOs have
456 been reported to home to lymph node like wild type, unlike our results here and in a
457 previous paper (Greenberg, Yu et al. 2013, Waite, Vardhana et al. 2013, Vaeth, Yang et
458 al. 2017). (2) Maximal T cell velocity in the lymph node requires the action of the integrin
459 LFA-1 and the chemokine receptor CCR7 (Davalos-Misslitz, Worbs et al. 2007, Katakai,
460 Habiro et al. 2013), which we have previously shown to be required for entry of T cells
461 into lymph nodes and to act in an Orai1-dependent manner (Greenberg, Yu et al. 2013).
462 Based upon these findings, blocking Orai1 would be expected to reduce CCR7 and LFA-
463 1 function during interstitial motility as well, resulting in a decrease in T cell velocity.

Instead, we find the opposite: Orai1 block leads to an increase in average cell velocity. The absence of any Orai1-dependent change in maximum velocity strongly suggests that CCR7 and LFA-1 do not act through Orai1 during motility in the lymph node. Regardless, any motility effects of LFA-1 and CCR7 are more than compensated by the reduction in pauses caused by Orai1 E106A expression. (3) Previous studies using unconfined open field motility assays have excluded a role for Orai1 in T cell motility (Svensson, McDowall et al. 2010, Kuras, Yun et al. 2012). Our experiments confirm that Orai1 block does not detectably affect unconfined motility; in contrast, our studies in reconstituted lymph nodes and in confined microchannels in vitro both exhibit Orai1-dependent effects. Others have shown that confined motility in vitro better recapitulates mechanisms of motility found in T cells in intact lymph nodes (Jacobelli, Friedman et al. 2010, Krummel, Bartumeus et al. 2016).

In conclusion, we reveal the existence of an Orai1-dependent cell motility program that leads to pausing of T cells moving within lymph nodes. Imaging with the newly developed genetically encoded Ca^{2+} indicator Salsa6f identifies local transient Ca^{2+} signaling events with the expected characteristics of Orai1 Ca^{2+} signals. We provide evidence that Orai1-dependent pauses in T cells are triggered in at least two different ways: by self-peptide MHC complexes displayed on the surface of APCs and by a novel cell intrinsic mechanism within the T cells themselves. Together these mechanisms generate motility patterns that promote efficient scanning for cognate antigens in the lymph node.

Acknowledgments

We thank Angel Zavala and Drs. Luette Forrest and Olga Safrina for expert assistance, excellent animal care and vivarium support, and Dr. Audrey Gerard, the Matthew Krummel Lab at UCSF, and the Christopher Hughes Lab at UCI for assistance in establishing the microchamber fabrication technique. We acknowledge the UC Irvine Institute for Clinical and Translational Science, and Dr. Jennifer Atwood of the Flow Core Facility supported by the UC Irvine Institute of Immunology.

Methods

Mice and antibodies

NOD.Cg-*Prkdc*^{scid}*B2m*^{tm1Unc}/J (NOD.SCID.β2) and NOD.CB17-*Prkdc*^{scid}/J (NOD.SCID) mice obtained from Jackson Laboratory (Stock #002570 and #001303) were housed and monitored in a selective pathogen-free environment with sterile food and water in the animal housing facility at the University of California, Irvine. NOD.SCID.β2 mice were reconstituted with human peripheral blood leukocytes (PBLs) as described previously (Mosier, Gulizia et al. 1988). A total of 3×10^7 human PBLs were injected i.p., and experiments were performed three weeks later. To inhibit NK cell activity, NOD.SCID mice were i.p. injected with 20 µL anti-NK cell antibody (rabbit anti-Asialo GM1, Wako Chemicals, Irvine, CA) according to manufacturer's instructions 3-4 days before adoptive transfer of human T cells. Mice used were between 8 and 18 weeks of age. The Salsa6f$^{LSL/LSL}$ (tdTomato-V5-GCaMP6f) mouse strain was generated in the C57BL/6N background, as described in the accompanying manuscript, and subsequently crossed to homozygotic CD4-Cre mice (JAX #017336) to generate CD4Cre$^{+/-}$ Salsa6f$^{+/-}$ mice (designated as CD4-Salsa6f$^{+/-}$ mice) expressing Salsa6f only in T cells. CD4Cre$^{+/-}$ Salsa6f$^{+/-}$ mice were further bred to generate homozygotic CD4Cre$^{+/-}$ Salsa6f$^{+/+}$ mice (CD4-Salsa6f$^{+/+}$ mice) for increased Salsa6f expression and fluorescence. Age- and sex-matched C57BL/6J mice from Jackson Laboratory (stock #000664) were used as wildtype recipients of CD4-Salsa6f$^{+/+}$ T cells. To block TCR-MHC interactions, 2 mg of anti-MHC II (Clone Y3P) and 2 mg of anti-MHC I (Clone AF6-88.5.5.3) or 4 mg of IgG2a Isotype control (Clone: C1.18.4) antibodies (Bio X cell) were injected into CD4-Salsa6f$^{+/+}$ litter mates (i.p) 48 hr before imaging.

516

517 **Human T cell preparation for imaging**

518 Human PBMCs were isolated from blood of voluntary healthy donors by Histopaque-1077
519 (1.077 g/mL; Sigma, St. Louis, MO) density gradient centrifugation, and human T cells
520 isolated using the appropriate EasySep T Cell Isolation Kit (StemCell Technologies).
521 Purified human T cells were rested overnight in complete RPMI, then transfected by
522 nucleofection (Lonza, Walkersville, MD), using the high-viability "U-014" protocol.
523 Enhanced green fluorescent protein (eGFP)-tagged wildtype Orai1, eGFP-tagged Orai1-
524 E106A mutant, Salsa6f (tdTomato-V5-GCaMP6f construct), or empty vector control were
525 transfected as indicated. Human T cells were used for experiments 3-48 hr after
526 transfection. CMTMR control T cells were prepared by labelling with 10 μM CellTracker
527 CMTMR dye (Invitrogen, Carlsbad, CA) for 10 min at 37 °C. For in vivo imaging 10 million
528 human T cells were injected into NOD.SCID.β2 or NOD.SCID mice as indicated. For in
529 vitro imaging experiments, T cells were rested for 3-4 hr in complete RPMI, then washed
530 and activated on plate-bound αCD3 and αCD28 (Tonbo Biosciences, San Diego, CA) in
531 2.5 ng/mL recombinant human IL-2 (BioLegend, San Diego, CA), and imaged 24-48 hr
532 after transfection.

533

534 **Mouse T cell preparation for imaging**

535 Single cell suspensions of mouse lymphocytes were prepared by mechanical dissociation
536 of spleen and lymph nodes and passing through 70 μm filter. $CD4^+$ T cells were isolated
537 using the EasySep T Cell Isolation Kit (StemCell Technologies) according to
538 manufacturer's instructions. The purity of isolated cells was confirmed to be >95% by flow

539 cytometry. To compare motility characteristics, CD4-Salsa6f$^{+/+}$ and CD4-Cre control cells
540 were labeled with 10 μM CellTrace Yellow or CellTrace Violet, respectively, for 20 min at
541 37^0 C. To measure Ca^{2+} during T cell motility, unlabeled CD4-Salsa6f$^{+/+}$ T cells were
542 adoptively transferred into wildtype recipients. A total of 3-10 million T cells were injected
543 into recipient mice in adoptive transfer experiments (*i.v*: tail-vein or retro-orbital). For
544 confocal imaging on open-field ICAM-1 coated coverslips, CD4+ T cells from CD4-
545 Salsa6f+/- mice were differentiated into Th1 cells using 25 ng/mL rmIL-12 (BioLegend),
546 10 μg/mL αmouse IL4 (Biolegend) for 4-6 days.
547
548 **Microchannel fabrication and imaging**
549 Microchannel fluidic devices were fabricated by a soft lithography technique with PDMS
550 (polydimethylsiloxane; Sylgard Elastomer 184 kit; Dow Corning, Auburn, MI) as described
551 (Jacobelli, Friedman et al. 2010, Gerard, Patino-Lopez et al. 2014). PDMS base and
552 curing agent were mixed 10:1 and poured onto the silicon master, then left overnight in
553 vacuum. Once the PDMS was set, it was baked at 55 °C for 1 hr and cooled at room
554 temperature. The embedded microchambers were then cut from the mold, and a cell well
555 was punched adjacent to entry into the channels. The PDMS cast and a chambered
556 coverglass (Nunc Lab-Tek, ThermoFisher, Grand Island, NY) were activated for two
557 minutes in a plasma cleaner (Harrick Plasma, Ithaca, NY), bonded together, then
558 incubated at 55 °C for 10 min. Prepared chambers were stored for up to 1 month before
559 use. Prior to imaging, microchambers placed in the plasma cleaner for 5 min under
560 vacuum and 1 min of activation, then coated with 5 μg/mL recombinant human ICAM-
561 1/CD54 Fc (R&D Systems, Minneapolis, MN) in PBS for at least 1 hr at 37 °C. The

562 microchambers were then washed three times with PBS, and T cells were loaded into cell
563 wells (3-5x10^5 cells resuspended in 10 µL) and incubated at 37 °C for at least 1 hr before
564 imaging.
565
566 **Confocal imaging and analysis**
567 Two different Olympus confocal microscopy systems were used to image T cells in vitro.
568 For experiments tracking T cell motility in microchambers, we used the self-contained
569 Olympus Fluoview FV10i-LIV, with a 473 nm diode laser for excitation and a 60x phase
570 contrast water immersion objective (NA 1.2). The FV10i-LIV contains a built-in incubator
571 set to 37 °C, together with a Tokai-Hit stagetop incubator to maintain local temperature
572 and humidity. T cells were imaged in RMPI adjusted to 2 mM Ca^{2+} and 2% FCS, and
573 mounted at least half an hour before imaging to allow for equilibration. Cells were imaged
574 at 20-sec intervals for 20-30 min, and the data analyzed using Imaris software. For Ca^{2+}
575 imaging of Salsa6f transfected T cells, we used a Fluoview FV3000RS confocal laser
576 scanning microscope, equipped with high speed resonance scanner and the IX3-ZDC2
577 Z-drift compensator. Diode lasers (488 and 561 nm) were used for excitation, and two
578 high sensitivity cooled GaAsP PMTs were used for detection of GCaMP6f and tdTomato.
579 Cells were imaged using the Olympus 40x silicone oil objective (NA 1.25), by taking 4
580 slice z-stacks at 1.5 µm/step, at 3 sec intervals, for up to 20 min. Temperature, humidity,
581 and CO_2 were maintained using a Tokai-Hit WSKM-F1 stagetop incubator. Data were
582 processed and analyzed using Imaris software.
583
584 **Two-photon imaging and analysis**

585 Multi-dimensional (x, y, z, time, emission wavelength) two-photon microscopy was
586 employed to image fluorescently labeled lymphocytes in explanted mouse lymph nodes,
587 as described (Miller, Wei et al. 2002, Matheu, Othy et al. 2015). The following
588 wavelengths were used to excite single or combinations of fluorophores: 900 nm to excite
589 eGFP and CMTMR; 800 nm to excite cell trace violet (Thermofisher C34557) and cell
590 trace yellow (Thermofisher, C34567); 920 nm to excite tdTomato and GCaMP6f;
591 Fluorescence emission was split by 484 nm & 538 nm dichroic mirrors into three detector
592 channels, used to visualize CellTrace Violet or second harmonic signal generated from
593 collagen in blue; GCaMP6f or eGFP-Orai1E106A transfected cells in green; tdTomato or
594 CellTrace Yellow or CMTMR-labelled cells in red. For imaging, lymph nodes were
595 oriented with the hilum away from the water dipping microscope objective (Olympus 20x,
596 NA 0.9 or Nikon 25x, NA 1.05) on an upright microscope (Olympus BX51). The node was
597 maintained at 36-37 °C by perfusion with medium (RPMI) bubbled with carbogen (95%
598 O_2 / 5% CO_2). For imaging of human T cells 3D image stacks of x=200 µm, y=162 µm,
599 and z=50 µm were sequentially acquired at 18-20 second intervals using MetaMorph
600 software (Molecular Devices, Sunnyvale, CA). For tracking adoptively transferred mouse
601 T cells, 3D image stacks of x=250 µm, y=250 µm, and z=20 or 52 µm (Voxel size 0.48
602 µm x 0.48 µm x 4 µm) were sequentially acquired at 5 or 12 second intervals respectively,
603 using image acquisition software Slidebook (Intelligent Imaging Innovations) as described
604 previously (Matheu, Othy et al. 2015). This volume collection was repeated for up to 40
605 min to create a 4D data set. For fast imaging of CD4-Salsa6f$^{+/+}$ lymph nodes, we acquired
606 2DT images of 300 µm x 300 µm (pixel size 0.65 x 0.65 µm) every 0.5 seconds. For
607 comparing Ca^{2+} transients in MHC blocking experiments, 3D image stacks of x=350 µm,

y=350 µm, and z=20 µm (Voxel size 0.65 µm x 0.65 µm x 4 µm) were sequentially acquired at 5 second intervals. Cell motility data were processed and analyzed using Imaris software (Bitplane USA, Concord, MA). A combination of manual and automatic tracking was used to generate highly accurate cell tracks. The x,y,z coordinates of the tracks were used to calculate speed, M.S.D, directionality ratio, motility coefficients, and to plot tracks as described previously (Gorelik and Gautreau 2014, Matheu, Othy et al. 2015). Calcium transient (sparkles and cell-wide) analysis and estimation of duration was performed as described previously (**eLIFE submission # 29-09-2017-lSRA-eLife-32417**). XYT data was processed to mask autofluorescent structures, and time was mapped on the Z axis for the purpose of Ca^{2+} transient identification. Ca^{2+} transients were identified in Imaris by a surface-based object identification approach, after manual thresholding of intensity, voxel size (>10) and 2-sec minimum duration. Objects were modeled as ellipsoids; X and Y diameter measurements of surfaces were used to calculated areas, and Z diameter (time) was used to estimate duration of Ca^{2+} transients. For MHC-block experiments to estimate the number and intensities of Ca^{2+} transients we utilized maximum intensity projections from 6 Z stacks. Integrated intensities were normalized to standard deviations of the green channel for comparison of brightness of Ca^{2+} transients.

Data analysis and statistical testing

Samples sizes were comparable to previous single cell analyses of motility (Jacobelli, Friedman et al. 2010, Greenberg, Yu et al. 2013, Gerard, Patino-Lopez et al. 2014). Each experiment used separate isolations of human T cells from different donors. With the

631 exception of instantaneous velocities in Figure 6C, each measurement corresponds to a
632 different cell. Mean ± standard error of the mean was used as a measure of the central
633 tendency of distributions. Video analysis was performed using Imaris software, Spots
634 analysis was used for tracking of cell velocity and Volumes analysis was used for
635 measuring total fluorescence intensity of GECI probes. To reduce selection bias in our
636 analysis of motility and trajectory, all clearly visible and live cells were tracked from each
637 video segment. The arrest coefficient is defined as fraction of time each cell had an
638 instantaneous velocity < 2 μm/min. The coefficient of variation was defined for each
639 individual cell as the standard deviation divided by the mean of its instantaneous velocity.
640 For Salsa6f imaging analysis, ratio (R) was calculated by total GCaMP6f intensity divided
641 by total tdTomato intensity, while initial ratio (R_0) was calculated by averaging the ratios
642 of the first five time points in each individual cell trace. Photobleaching of tdTomato
643 fluorescence intensity (20-30% decline) was corrected in ratio calculations, as a linear
644 function of time. Figures were generated using Prism 6 (GraphPad Software, San Diego,
645 CA) and Origin 5 (OriginLabs, Northampton, MA). Due to the expectation that individual
646 cells exhibit multiple motility modes, and to avoid assumptions concerning the shapes of
647 motility distributions, non-parametric statistical testing was performed (Mann-Whitney *U*
648 test, unpaired samples, two-tailed, Spearman's rank correlation). Differences with a *p*
649 value of ≤ 0.05 were considered significant: *$p \leq 0.05$; **$p < 0.01$; ***$p < 0.005$; ****$p <$
650 0.001. Similar distributions were compared using the Hodges-Lehmann median
651 difference value and 95% confidence intervals under the assumption that the starting
652 distributions had similar shapes.
653

References

Babich, A. and J. K. Burkhardt (2013). "Coordinate control of cytoskeletal remodeling and calcium mobilization during T-cell activation." Immunol Rev **256**(1): 80-94.

Bajenoff, M., J. G. Egen, L. Y. Koo, J. P. Laugier, F. Brau, N. Glaichenhaus and R. N. Germain (2006). "Stromal cell networks regulate lymphocyte entry, migration, and territoriality in lymph nodes." Immunity **25**(6): 989-1001.

Barr, V. A., K. M. Bernot, S. Srikanth, Y. Gwack, L. Balagopalan, C. K. Regan, D. J. Helman, C. L. Sommers, M. Oh-Hora, A. Rao and L. E. Samelson (2008). "Dynamic movement of the calcium sensor STIM1 and the calcium channel Orai1 in activated T-cells: puncta and distal caps." Mol Biol Cell **19**(7): 2802-2817.

Bhakta, N. R., D. Y. Oh and R. S. Lewis (2005). "Calcium oscillations regulate thymocyte motility during positive selection in the three-dimensional thymic environment." Nat Immunol **6**(2): 143-151.

Bousso, P. and E. Robey (2003). "Dynamics of CD8+ T cell priming by dendritic cells in intact lymph nodes." Nat Immunol **4**(6): 579-585.

Cahalan, M. D. and K. G. Chandy (2009). "The functional network of ion channels in T lymphocytes." Immunol Rev **231**(1): 59-87.

Cahalan, M. D. and I. Parker (2005). "Close encounters of the first and second kind: T-DC and T-B interactions in the lymph node." Semin Immunol **17**(6): 442-451.

Calloway, N., M. Vig, J. P. Kinet, D. Holowka and B. Baird (2009). "Molecular clustering of STIM1 with Orai1/CRACM1 at the plasma membrane depends dynamically on depletion of Ca2+ stores and on electrostatic interactions." Mol Biol Cell **20**(1): 389-399.

Davalos-Misslitz, A. C., T. Worbs, S. Willenzon, G. Bernhardt and R. Forster (2007). "Impaired responsiveness to T-cell receptor stimulation and defective negative selection of thymocytes in CCR7-deficient mice." Blood **110**(13): 4351-4359.

Dixit, N., I. Yamayoshi, A. Nazarian and S. I. Simon (2011). "Migrational guidance of neutrophils is mechanotransduced via high-affinity LFA-1 and calcium flux." J Immunol **187**(1): 472-481.

Donnadieu, E., G. Bismuth and A. Trautmann (1994). "Antigen recognition by helper T cells elicits a sequence of distinct changes of their shape and intracellular calcium." Curr Biol **4**(7): 584-595.

685 Dustin, M. L., S. K. Bromley, Z. Kan, D. A. Peterson and E. R. Unanue (1997). "Antigen receptor
686 engagement delivers a stop signal to migrating T lymphocytes." Proc Natl Acad Sci U S
687 A **94**(8): 3909-3913.
688 Feske, S. (2007). "Calcium signalling in lymphocyte activation and disease." Nat Rev Immunol
689 **7**(9): 690-702.
690 Feske, S., Y. Gwack, M. Prakriya, S. Srikanth, S. H. Puppel, B. Tanasa, P. G. Hogan, R. S.
691 Lewis, M. Daly and A. Rao (2006). "A mutation in Orai1 causes immune deficiency by
692 abrogating CRAC channel function." Nature **441**(7090): 179-185.
693 Fischer, U. B., E. L. Jacovetty, R. B. Medeiros, B. D. Goudy, T. Zell, J. B. Swanson, E. Lorenz,
694 Y. Shimizu, M. J. Miller, A. Khoruts and E. Ingulli (2007). "MHC class II deprivation
695 impairs CD4 T cell motility and responsiveness to antigen-bearing dendritic cells in vivo."
696 Proc Natl Acad Sci U S A **104**(17): 7181-7186.
697 Friedl, P. and B. Weigelin (2008). "Interstitial leukocyte migration and immune function." Nat
698 Immunol **9**(9): 960-969.
699 Gerard, A., G. Patino-Lopez, P. Beemiller, R. Nambiar, K. Ben-Aissa, Y. Liu, F. J. Totah, M. J.
700 Tyska, S. Shaw and M. F. Krummel (2014). "Detection of rare antigen-presenting cells
701 through T cell-intrinsic meandering motility, mediated by Myo1g." Cell **158**(3): 492-505.
702 Germain, R. N., E. A. Robey and M. D. Cahalan (2012). "A decade of imaging cellular motility
703 and interaction dynamics in the immune system." Science **336**(6089): 1676-1681.
704 Gorelik, R. and A. Gautreau (2014). "Quantitative and unbiased analysis of directional
705 persistence in cell migration." Nat Protoc **9**(8): 1931-1943.
706 Greenberg, M. L., Y. Yu, S. Leverrier, S. L. Zhang, I. Parker and M. D. Cahalan (2013). "Orai1
707 function is essential for T cell homing to lymph nodes." J Immunol **190**(7): 3197-3206.
708 Hartzell, C. A., K. I. Jankowska, J. K. Burkhardt and R. S. Lewis (2016). "Calcium influx through
709 CRAC channels controls actin organization and dynamics at the immune synapse." Elife
710 **5**.
711 Hou, X., L. Pedi, M. M. Diver and S. B. Long (2012). "Crystal structure of the calcium release-
712 activated calcium channel Orai." Science **338**(6112): 1308-1313.
713 Jacobelli, J., R. S. Friedman, M. A. Conti, A. M. Lennon-Dumenil, M. Piel, C. M. Sorensen, R. S.
714 Adelstein and M. F. Krummel (2010). "Confinement-optimized three-dimensional T cell
715 amoeboid motility is modulated via myosin IIA-regulated adhesions." Nat Immunol
716 **11**(10): 953-961.
717 Katakai, T., K. Habiro and T. Kinashi (2013). "Dendritic cells regulate high-speed interstitial T
718 cell migration in the lymph node via LFA-1/ICAM-1." J Immunol **191**(3): 1188-1199.

719 Khan, O., M. Headley, A. Gerard, W. Wei, L. Liu and M. F. Krummel (2011). "Regulation of T
720 cell priming by lymphoid stroma." PLoS One **6**(11): e26138.
721 Korkotian, E., E. Oni-Biton and M. Segal (2017). "The role of the store-operated calcium entry
722 channel Orai1 in cultured rat hippocampal synapse formation and plasticity." J Physiol
723 **595**(1): 125-140.
724 Krummel, M. F., F. Bartumeus and A. Gerard (2016). "T cell migration, search strategies and
725 mechanisms." Nat Rev Immunol **16**(3): 193-201.
726 Krummel, M. F., R. S. Friedman and J. Jacobelli (2014). "Modes and mechanisms of T cell
727 motility: roles for confinement and Myosin-IIA." Curr Opin Cell Biol **30C**: 9-16.
728 Kuras, Z., Y. H. Yun, A. A. Chimote, L. Neumeier and L. Conforti (2012). "KCa3.1 and TRPM7
729 channels at the uropod regulate migration of activated human T cells." PLoS One **7**(8):
730 e43859.
731 Liou, J., M. L. Kim, W. D. Heo, J. T. Jones, J. W. Myers, J. E. Ferrell, Jr. and T. Meyer (2005).
732 "STIM is a Ca2+ sensor essential for Ca2+-store-depletion-triggered Ca2+ influx." Curr
733 Biol **15**(13): 1235-1241.
734 Lioudyno, M. I., J. A. Kozak, A. Penna, O. Safrina, S. L. Zhang, D. Sen, J. Roos, K. A.
735 Stauderman and M. D. Cahalan (2008). "Orai1 and STIM1 move to the immunological
736 synapse and are up-regulated during T cell activation." Proc Natl Acad Sci U S A **105**(6):
737 2011-2016.
738 Luik, R. M., M. M. Wu, J. Buchanan and R. S. Lewis (2006). "The elementary unit of store-
739 operated Ca2+ entry: local activation of CRAC channels by STIM1 at ER-plasma
740 membrane junctions." J Cell Biol **174**(6): 815-825.
741 Matheu, M. P., S. Othy, M. L. Greenberg, T. X. Dong, M. Schuijs, K. Deswarte, H. Hammad, B.
742 N. Lambrecht, I. Parker and M. D. Cahalan (2015). "Imaging regulatory T cell dynamics
743 and CTLA4-mediated suppression of T cell priming." Nat Commun **6**: 6219.
744 Maus, M., M. Cuk, B. Patel, J. Lian, M. Ouimet, U. Kaufmann, J. Yang, R. Horvath, H. T. Hornig-
745 Do, Z. M. Chrzanowska-Lightowlers, K. J. Moore, A. M. Cuervo and S. Feske (2017).
746 "Store-Operated Ca2+ Entry Controls Induction of Lipolysis and the Transcriptional
747 Reprogramming to Lipid Metabolism." Cell Metab.
748 Mempel, T. R., S. E. Henrickson and U. H. Von Andrian (2004). "T-cell priming by dendritic cells
749 in lymph nodes occurs in three distinct phases." Nature **427**(6970): 154-159.
750 Miller, M. J., A. S. Hejazi, S. H. Wei, M. D. Cahalan and I. Parker (2004). "T cell repertoire
751 scanning is promoted by dynamic dendritic cell behavior and random T cell motility in the
752 lymph node." Proc Natl Acad Sci U S A **101**(4): 998-1003.

753 Miller, M. J., S. H. Wei, I. Parker and M. D. Cahalan (2002). "Two-photon imaging of lymphocyte
754 motility and antigen response in intact lymph node." Science **296**(5574): 1869-1873.
755 Moreau, H. D., F. Lemaitre, K. R. Garrod, Z. Garcia, A. M. Lennon-Dumenil and P. Bousso
756 (2015). "Signal strength regulates antigen-mediated T-cell deceleration by distinct
757 mechanisms to promote local exploration or arrest." Proc Natl Acad Sci U S A **112**(39):
758 12151-12156.
759 Morley, S. C. (2013). "The actin-bundling protein L-plastin supports T-cell motility and
760 activation." Immunol Rev **256**(1): 48-62.
761 Mosier, D. E., R. J. Gulizia, S. M. Baird and D. B. Wilson (1988). "Transfer of a functional
762 human immune system to mice with severe combined immunodeficiency." Nature
763 **335**(6187): 256-259.
764 Mrass, P., J. Petravic, M. P. Davenport and W. Weninger (2010). "Cell-autonomous and
765 environmental contributions to the interstitial migration of T cells." Semin Immunopathol
766 **32**(3): 257-274.
767 Negulescu, P. A., T. B. Krasieva, A. Khan, H. H. Kerschbaum and M. D. Cahalan (1996).
768 "Polarity of T cell shape, motility, and sensitivity to antigen." Immunity **4**(5): 421-430.
769 Petrie, R. J., A. D. Doyle and K. M. Yamada (2009). "Random versus directionally persistent cell
770 migration." Nat Rev Mol Cell Biol **10**(8): 538-549.
771 Prakriya, M., S. Feske, Y. Gwack, S. Srikanth, A. Rao and P. G. Hogan (2006). "Orai1 is an
772 essential pore subunit of the CRAC channel." Nature **443**(7108): 230-233.
773 Roos, J., P. J. DiGregorio, A. V. Yeromin, K. Ohlsen, M. Lioudyno, S. Zhang, O. Safrina, J. A.
774 Kozak, S. L. Wagner, M. D. Cahalan, G. Velicelebi and K. A. Stauderman (2005).
775 "STIM1, an essential and conserved component of store-operated Ca2+ channel
776 function." J Cell Biol **169**(3): 435-445.
777 Schaff, U. Y., N. Dixit, E. Procyk, I. Yamayoshi, T. Tse and S. I. Simon (2010). "Orai1 regulates
778 intracellular calcium, arrest, and shape polarization during neutrophil recruitment in
779 shear flow." Blood **115**(3): 657-666.
780 Shultz, L. D., P. A. Schweitzer, S. W. Christianson, B. Gott, I. B. Schweitzer, B. Tennent, S.
781 McKenna, L. Mobraaten, T. V. Rajan, D. L. Greiner and et al. (1995). "Multiple defects in
782 innate and adaptive immunologic function in NOD/LtSz-scid mice." J Immunol **154**(1):
783 180-191.
784 Stefanova, I., J. R. Dorfman and R. N. Germain (2002). "Self-recognition promotes the foreign
785 antigen sensitivity of naive T lymphocytes." Nature **420**(6914): 429-434.

786 Svensson, L., A. McDowall, K. M. Giles, P. Stanley, S. Feske and N. Hogg (2010). "Calpain 2
787 controls turnover of LFA-1 adhesions on migrating T lymphocytes." PLoS One **5**(11):
788 e15090.
789 Vaeth, M., J. Yang, M. Yamashita, I. Zee, M. Eckstein, C. Knosp, U. Kaufmann, P. Karoly Jani,
790 R. S. Lacruz, V. Flockerzi, I. Kacskovics, M. Prakriya and S. Feske (2017). "ORAI2
791 modulates store-operated calcium entry and T cell-mediated immunity." Nat Commun **8**:
792 14714.
793 Vig, M., A. Beck, J. M. Billingsley, A. Lis, S. Parvez, C. Peinelt, D. L. Koomoa, J. Soboloff, D. L.
794 Gill, A. Fleig, J. P. Kinet and R. Penner (2006). "CRACM1 multimers form the ion-
795 selective pore of the CRAC channel." Curr Biol **16**(20): 2073-2079.
796 Waite, J. C., S. Vardhana, P. J. Shaw, J. E. Jang, C. A. McCarl, T. O. Cameron, S. Feske and
797 M. L. Dustin (2013). "Interference with Ca(2+) release activated Ca(2+) (CRAC) channel
798 function delays T-cell arrest in vivo." Eur J Immunol **43**(12): 3343-3354.
799 Wei, S. H., I. Parker, M. J. Miller and M. D. Cahalan (2003). "A stochastic view of lymphocyte
800 motility and trafficking within the lymph node." Immunol Rev **195**: 136-159.
801 Wei, S. H., O. Safrina, Y. Yu, K. R. Garrod, M. D. Cahalan and I. Parker (2007). "Ca2+ signals
802 in CD4+ T cells during early contacts with antigen-bearing dendritic cells in lymph node."
803 J Immunol **179**(3): 1586-1594.
804 Wu, M. M., E. D. Covington and R. S. Lewis (2014). "Single-molecule analysis of diffusion and
805 trapping of STIM1 and Orai1 at endoplasmic reticulum-plasma membrane junctions."
806 Mol Biol Cell **25**(22): 3672-3685.
807 Yeromin, A. V., S. L. Zhang, W. Jiang, Y. Yu, O. Safrina and M. D. Cahalan (2006). "Molecular
808 identification of the CRAC channel by altered ion selectivity in a mutant of Orai." Nature
809 **443**(7108): 226-229.
810 Zhang, S. L., A. V. Yeromin, X. H. Zhang, Y. Yu, O. Safrina, A. Penna, J. Roos, K. A.
811 Stauderman and M. D. Cahalan (2006). "Genome-wide RNAi screen of Ca(2+) influx
812 identifies genes that regulate Ca(2+) release-activated Ca(2+) channel activity." Proc
813 Natl Acad Sci U S A **103**(24): 9357-9362.
814 Zhang, S. L., Y. Yu, J. Roos, J. A. Kozak, T. J. Deerinck, M. H. Ellisman, K. A. Stauderman and
815 M. D. Cahalan (2005). "STIM1 is a Ca2+ sensor that activates CRAC channels and
816 migrates from the Ca2+ store to the plasma membrane." Nature **437**(7060): 902-905.

817

Figure Legends

Figure 1. **Effects of expressing Orai1-E106A on human T cells.** (**A**) Averaged thapsigargin-induced Ca^{2+} entry, measured by fura-2, in activated human $CD4^+$ T cells transfected with eGFP-Orai1-E106A (left) or empty vector control (EV, right, n = 133 cells); eGFP-E106A transfected cells were grouped into two populations, either eGFP-$E106A^{hi}$ with high eGFP fluorescence (solid squares, n = 43 cells) or eGFP-$E106A^{lo}$ with no detectable eGFP fluorescence (empty squares, n = 115 cells); bars represent SEM. (**B**) Primary human $CD4^+$ and $CD8^+$ T cells were transfected with eGFP-E106A, then uniformly labeled with the fluorescent cell tracker dye CMTMR and co-cultured with SEB-pulsed primary human dendritic cells from the same donor; proliferation was assessed after 72 hr by CMTMR dilution as measured by flow cytometry. (**C**) Human $CD3^+$ T cells were transfected with eGFP-E106A and expression level was measured 3 hr post-transfection before adoptive transfer into reconstituted NOD.SCI.β2 mice; cells were recovered from lymph nodes 18 hr later and eGFP fluorescence was used to measure homing to lymph nodes.

Figure 1-figure supplement 1. **Protocol for homing and two-photon imaging of transfected human $CD3^+$ T cells in reconstituted NOD.SCID.β2 mouse lymph node.**

Figure 2. **Orai1 block increases human T cell motility within reconstituted NOD.SCID.β2 lymph nodes.** (**A**) Two-photon microscopy of migrating human T cells, showing eGFP-E106A transfected cells in green and CMTMR-labeled mock transfected cells in red, within intact mouse lymph node 18 hr after adoptive co-transfer of $5x10^6$ of each cell type. (**B**) Average cell velocities of eGFP-$E106A^{hi}$ (n = 50) versus CMTMR-labeled control (n = 71) T cells; bars represent mean ± SEM, data from independent experiments using 4 different donors (12.8 ± 0.5 μm/min vs. 11.1 ± 0.5 μm/min for $E106A^{hi}$ vs CMTMR cells, p = 0.0268). (**C**) Maximum and minimum cellular instantaneous velocities of eGFP-$E106A^{hi}$ (green) versus CMTMR-labeled (red) control T cells. (Hodges-Lehmann median difference of -0.21 μm/min, -2.82 to 2.16 μm/min 95% confidence interval for maximum velocity and -0.36 μm/min, -1.02 to 0.36 μm/min 95% confidence interval for minimum velocity) (**D**) Superimposed tracks with their origins normalized to the starting point. Cells were tracked for more than 20 min. n = 111

(CMTMR), n=58 (eGFP-E106A^{hi}) (**E**) Directionality ratio (displacement / distance) over elapsed time. For Orai1-blocked cells in green, tau = 397 sec; vs CMTMR controls in red, tau = 238 sec, n = 49 time points. (**F**) Histogram of turn angles in eGFP-E106A^{hi} (green) and CMTMR controls (red). Mean ± SEM, 74.5 ± 1.0 degrees for Orai1 blocked cells vs 86.5 ± 1.5 degrees for CMTMR controls, p = 0.0001, two-tailed T test. (**G**) Arrest coefficients of eGFP-E106A^{hi} compared with CMTMR-labeled control T cells, defined as fraction of time with instantaneous velocity < 2 μm/min. (For Orai1-blocked cells in green, 0.02 ± 0.01; vs. CMTMR controls in red, 0.12 ± 0.03, p = 0.0406) (**H**) Frequency distribution of average cell velocities for eGFP-E106A^{hi} (top) and CMTMR-labeled control T cells (bottom), cells with average velocity < 7 μm/min are highlighted in gray; tick marks denote the center of every other bin. (**I,J**) Average cell velocities (**I**) and arrest coefficients (**J**) of eGFP-E106A^{hi} (green, n = 102) vs CMTMR-labeled control (red, n = 278) human T cells in NK cell depleted immunodeficient mouse lymph nodes. Average cell velocities: 11.0 ± 0.5 μm/min vs. 8.8 ± 0.3 μm/min, p = 0.0004; Arrest coefficients: 0.10 ± 0.02 vs. 0.16 ± 0.01, p = 0.0516 for E106A^{hi} vs CMTMT cells; bars represent mean ± SEM, data from independent experiments using 8 different donors, *** = p < 0.005.

Figure 3. **Orai1 block reduces frequency of pausing during human T cell motility in vitro.** (**A,B**) Confocal microscopy of eGFP-E106A transfected human CD4^{+} T cells in microfabricated channels 7 μm high by 8 μm wide, showing two individual eGFP-E106A^{hi} T cells (**A**) and two eGFP-E106A^{lo} T cells (**B**), each circled in red in the first frame; individual images taken 1 min apart, scale bar = 10 μm. (**C**) Comparison of average cell velocities of eGFP-E106A transfected T cells (eGFP-E106A^{hi} cells in green, n = 102; eGFP-E106A^{lo} cells in gray, n =131; 14.2 ± 0.6 μm/min vs. 10.9 ± 0.5 μm/min, p < 0.0001 for E106A^{hi} vs E106A^{lo} cells) and eGFP-Orai1 transfected control T cells (eGFP-Orai1^{hi} cells in green, n = 43; eGFP-Orai1^{lo} cells in gray, n = 76; 10.7 ± 0.8 μm/min vs. 10.5 ± 0.8 μm/min for Orai1^{hi} vs Orai1^{lo} cells; Hodges-Lehmann median difference of -0.84 μm/min, -2.96 to 1.28 μm/min 95%CI); bars represent mean ± SEM, data from independent experiments using 5 different donors. (**D**) Frequency distribution of average cell velocities of eGFP-E106A^{hi} (top) and eGFP-E106A^{lo} (bottom) human T cells, cells with average velocity < 7 μm/min are highlighted in gray; tick marks denote the center of every other

bin. (**E**) Arrest coefficients of eGFP-E106A^{hi} vs eGFP-E106A^{lo} human T cells, defined as fraction of time each individual cell had an instantaneous velocity < 2 μm/min (0.05 ± 0.01 vs. 0.08 ± 0.01 for E106A^{hi} vs E106A^{lo} cells, p = 0.0015); (**F**) Variance in velocity of eGFP-E106A^{hi} vs eGFP-E106A^{lo} human T cells, coefficient of variation is calculated by standard deviation divided by the mean of instantaneous velocity for each individual cell (39.5 ± 1.9 % vs. 45.1 ± 1.6 % for E106A^{hi} vs E106A^{lo} cells, p = 0.0138);. (**G**) Duration of pauses for eGFP-E106A^{hi} vs eGFP-E106A^{lo} human T cells (Hodges-Lehmann median difference of 0 seconds, -8.43 to 4.71 seconds 95%CI for E106A^{hi} vs E106A^{lo} cells); bars represent mean ± SEM, * = p < 0.05, ** = p < 0.01, *** = p < 0.005, **** = p < 0.001.

Figure 4. **Tracking Ca^{2+} signals in human T cells in vitro with Salsa6f.** (**A,C**) Confocal microscopy of Salsa6f transfected human CD4$^+$ T cells in ICAM-1 coated microchannels 7 μm high by 8 μm wide (**A, Video 5**) and open space (**C, Video 6**), showing merged red (tdTomato), green (GCaMP6f), and DIC channels; circular structures shown in (**C**) are support pillars part of the PDMS chamber; scale bar = 10 μm, time = sec;. (**B,D**) Total intensity tracings of GCaMP6f (green) and tdTomato (red) fluorescence, G/R ratio (orange), and speed (black), for corresponding T cells shown in (**A**) and (**C**); data representative of independent experiments from three different donors.

Figure 5. **Spontaneous Ca^{2+} signals during human T cell motility in vitro are correlated with reduced velocity.** (**A,B**) Sample tracks from Salsa6f-transfected human T cells in microchannels, with intracellular Ca^{2+} levels as G/R ratios for each time point, normalized to zero-time (orange), overlaid with instantaneous cell velocity (black), cells in (**A**) have stable Ca^{2+} levels, cells in (**B**) show brief Ca^{2+} transients (arrowheads) or sustained Ca^{2+} signaling (gray highlights). (**C**) Instantaneous velocity of Salsa6f-transfected human T cells in microchannels during elevated cytosolic Ca^{2+} levels (red) and during basal Ca^{2+} levels (green); n = 22 cells, data from independent experiments using three different donors; **** = p < 0.001. (**D**) Scatter plot of Salsa transfected human T cells in microchannels, instantaneous cell velocity versus normalized G/R ratio for each individual time point analyzed; red numbers in each quadrant show percent of time points, split by 1.10 normalized G/R ratio and 10 μm/min; n = 4081 points. (**E**) Mean track velocity of eGFP-E106A transfected human T cells, comparing eGFP-E106A^{hi} (green) versus

eGFP-E106A^{lo} T cells (gray) in confined microchannels vs open space; n = 30, 44, 33, and 62 cells, respectively (15.4 ± 1.2 μm/min vs. 11.3 ± 1.0 μm/min for E106A^{hi} vs E106A^{lo} cells in microchannels; p = 0.0099 and 12.0 ± 1.0 μm/min vs. 12.2 ± 0.7 μm/min for E106A^{hi} vs E106A^{lo} cells in open space; Hodges-Lehmann median difference of 0.15 μm/min, -2.46 to 2.40 μm/min 95%CI); bars represent mean ± SEM, data from independent experiments using two different donors, * = p < 0.05, ** = p < 0.01. (**F**) Scatter plot of Salsa transfected human T cells in open space, instantaneous cell velocity versus GCaMP6f/tdTomato R/R$_0$ for each individual time point analyzed; red numbers in each quadrant show percent of cells, split by 1.10 normalized G/R ratio and 10 μm/min; n = 723 points.

Figure 5-figure supplement 1. Tracking cell motility and Ca^{2+} signals in CD4-Salsa6f$^{+/-}$ T cells on ICAM coated coverslips. (**A**) Confocal microscopy of CD4-Salsa6f$^{+/-}$ Th1 cells on open-field ICAM-1 coated coverslips showing merged red (tdTomato) and green (GCaMP6f) channels at three different time points. Scale bar 10 μm. * indicates movement of one cell. (**B**) Recordings of GCaMP6f (green), tdTomato (red) fluorescence, G/R ratio (orange), and speed (black), for corresponding T cell shown in (**A**). (**C**) Average cell velocities of CD4-Salsa6f$^{+/-}$ Th1 cells on 5 μg/ml ICAM-1 coated coverslips (n = 52 cells, 2 independent experiments). (**D**) Scatter plot showing instantaneous cell velocity versus GCaMP6f/tdTomato (G/R) ratio for each individual time point analyzed; numbers show percent of time points, split by 10 μm/min, as in **Figure 8 D,F**; n = 5289 points.

Figure 6. Motility of Salsa6f T cells in lymph node following adoptive transfer. CD4-Cre and CD4-Salsa6f$^{+/+}$ cells are shown in teal and in red, respectively. (**A**) Experimental design to characterize homing and motility of CD4-Salsa6f$^{+/+}$ cells. CTV-labeled CD4-Cre cells and CTY-labeled CD4-Salsa6f$^{+/+}$ cells (1:1) were adoptively transferred into wildtype mice, 18 hr prior to LN harvesting. (**B**) Paired numbers of CTV$^+$ and CTY$^+$ cells recovered from lymph nodes (p = 0.65, Mann Whitney test). (**C**) Representative median filtered, maximum intensity projection image showing simultaneously imaged CD4-Cre and CD4-Salsa6f$^{+/+}$ cells the lymph node, scale bar = 30 μm. See **Video 1**. (**D**) Superimposed

tracks with their origins normalized to the starting point. Cells were tracked for more than 20 min. n = 140. See Video 2. (**E**) Frequency distribution of instantaneous velocities; arrows indicate median, tick marks at the center of every other bin (n > 14,800, 3 independent experiments). (**F**) Scatter plot showing mean track speed, black bars indicate overall mean values (11.1 ± 0.4 and 10.7 ± 0.4 μm/min, for CD4-Cre and CD4-Salsa6f$^{+/+}$ cells respectively, p = 0.69; n= 140). (**G**) Directionality ratio (displacement / distance) over elapsed time tau = 461.2 sec for CD4-Cre in teal; vs tau = 474.1 sec for CD4- Salsa6f$^{+/+}$ in red. n= 217 time points. (**H**) MSD vs time, plotted on a log-log scale. (**I**) Measured motility coefficient from 140 tracks (35.1 ± 3.2 vs 39.4 ± 3.9 μm^2/min for CD4-Cre and CD4-Salsa6f$^{+/+}$ cells , p = 0.65).

Figure 7. Suppression of motility during spontaneous Ca^{2+} transients. (**A**) Median filtered, maximum intensity projection showing cytosolic labeling (exclusion of Salsa6f from the nucleus) in adoptively transferred CD4-Salsa6f$^{+/+}$ cells (red) in the lymph node of wildtype recipients. Autofluorescent structures appear as yellow bodies. Scale bar = 20 μm. See **Video 2**. (**B**) Scatterplot of instantaneous 3D velocity vs ratio of GCaMP6f (green) to tdTomato (red) fluorescence intensity (r = -0.24, Spearman's rank correlation, p < 0.0001, n = 4490 pairs). (**C**) Image sequence showing a migrating T cell and calcium transient from (**A**). Top row: TdTomato signal is shown in grayscale, overlaid with GCaMP6f signals in green. Scale bar = 10 μm. Center row: Heat map of Green / Red ratios matched to corresponding images in the top row. Arrows indicate local Ca^{2+} transient. Bottom row: inverted bar graph showing corresponding instantaneous 3D velocities. Asterisk marks a pause in cell motility. (**D**) Representative track from CD4-Salsa6f$^{+/+}$ T cells in lymph nodes, showing intracellular Ca^{2+} levels measured by G/R ratio (orange) on left Y-axis and instantaneous 3D velocity (gray) on right Y-axis. (**E**) Averaged time course of the instantaneous 3D velocity (gray trace, right Y-axis) aligned by the corresponding rise in Salsa6f G/R ratio (orange, left Y-axis). The velocity minimum at time = 5 sec-is significantly lower than a baseline from -30 to -10 sec (p<0.0001 two-tailed T-test, n = 39 cells).

Figure 8. T cell Ca^{2+} transients in the steady-state lymph node. (**A**) Calcium history map of steady-state lymph node. Maximum intensity YT projection of 1200 processed

970 green channel time points showing localized sparkles (white arrows) and cell-wide global
971 Ca^{2+} transients (magenta arrows). Scale bar = 50 μm along Y axis, 50 sec along T axis.
972 See **Video 3**. (**B**) Frequency distribution of the area of local Ca^{2+} signals. (**C**) Frequency
973 distribution of the duration of local Ca^{2+} signals.

974 **Figure 9**. **MHC block and Ca^{2+} transients in steady state lymph nodes**. (**A**) The
975 frequency of cell-wide and local (sparkles) Ca^{2+} transients in CD-Salsa6f$^{+/+}$ lymph nodes
976 48 hr after injection of MHC class I and II blocking antibodies (MHC), isotype control
977 antibody (ITC), or no antibody (Con). Red bars indicate mean values. For MHC-blocked
978 compared to ITC, the relative event frequencies were, for cell-wide: 314 ± 38 vs 553 ± 77,
979 mean ± SEM, p = 0.06; for sparkles: 532 ± 44 vs 1343 ± 272, mean ± SEM, p = 0.02,
980 Mann Whitney test. (**B,C**) Integrated green channel intensities of Ca^{2+} transients
981 normalized to SD of green channel for cell-wide events (**B**) and for sparkles (**C**). Red bars
982 indicate mean values. For MHC-blocked vs ITC, the relative amplitudes were, for cell-
983 wide (**B**): 321 ± 14 vs 350 ± 15, mean ± SEM; sparkles (**C**): 32 ± 2 vs 37 ± 2, mean ±
984 SEM. (**D-G**) Representative thresholded images showing cell-wide and local Ca^{2+}
985 transients, 48 hr after treatment with anti MHC I and II or ITC antibody. The area of the
986 imaging field analyzed is indicated. Scale bar = 100 μm.

987

988

989 **Figure 1**

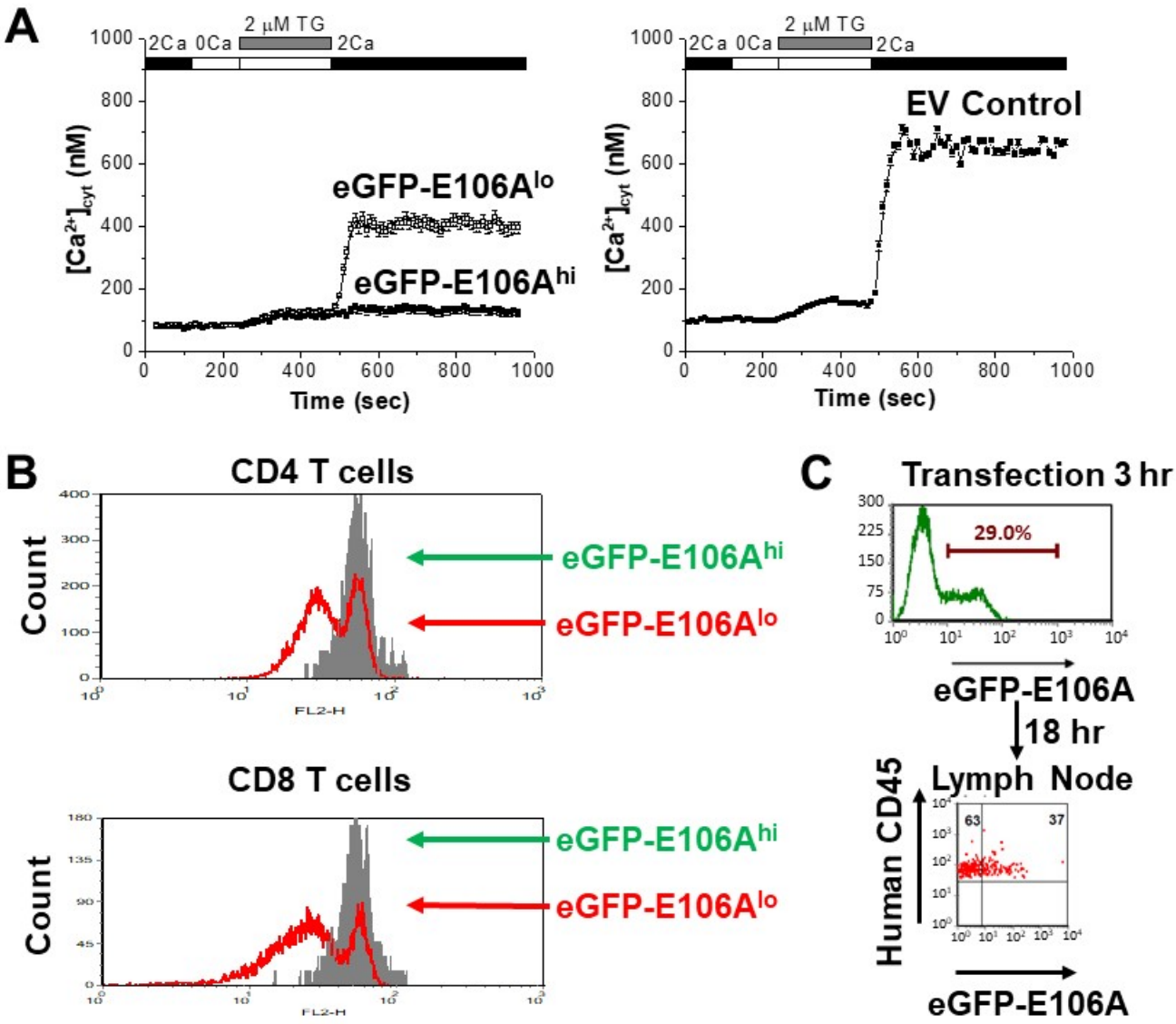

990

991

992 **Figure 1 Supplement 1**

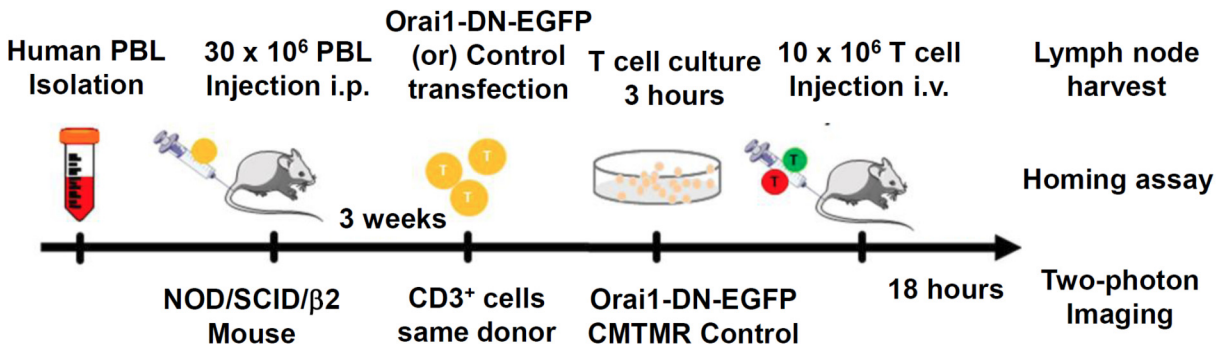

993

994

995 **Figure 2**

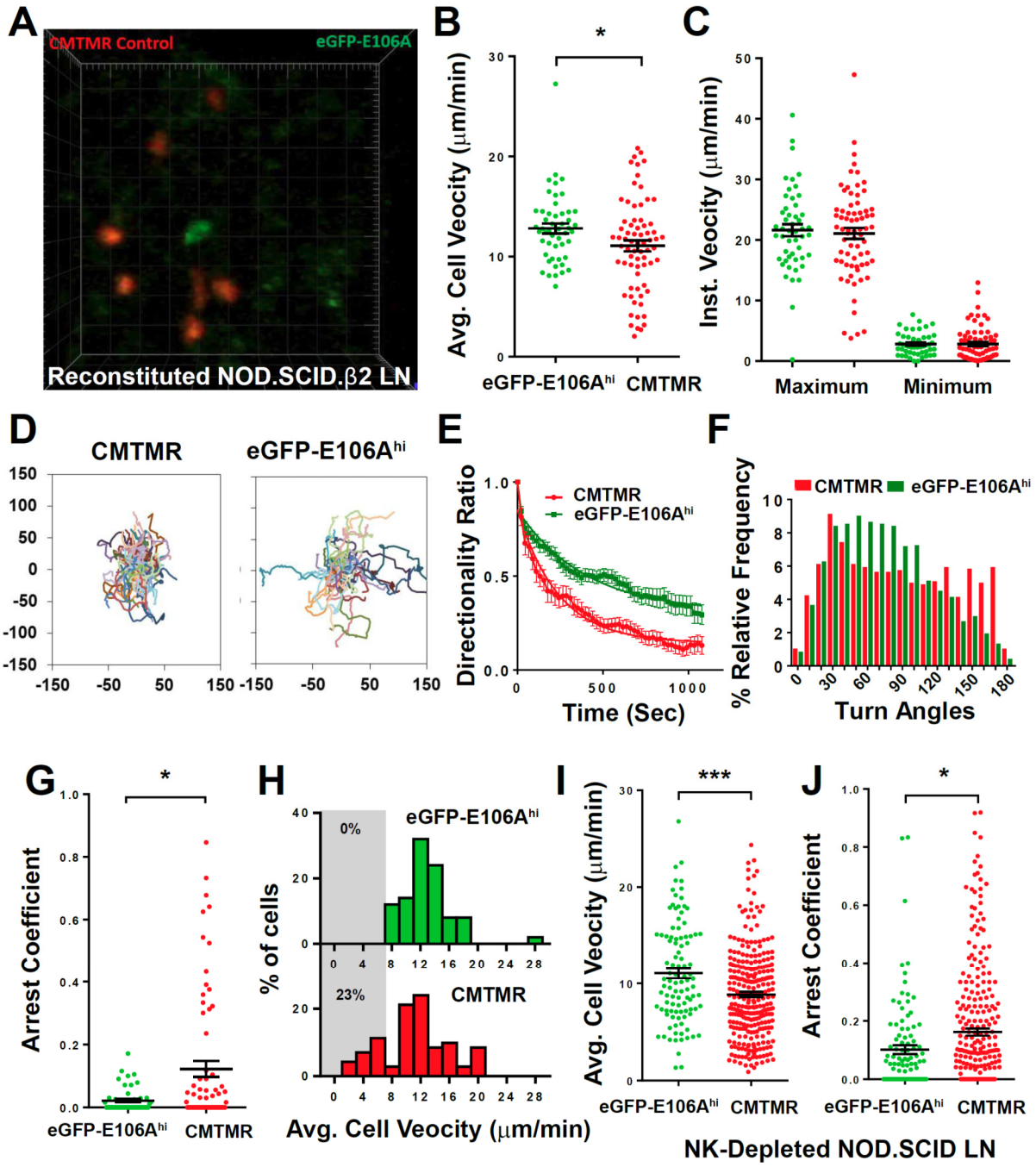

996

997

998 **Figure 3**

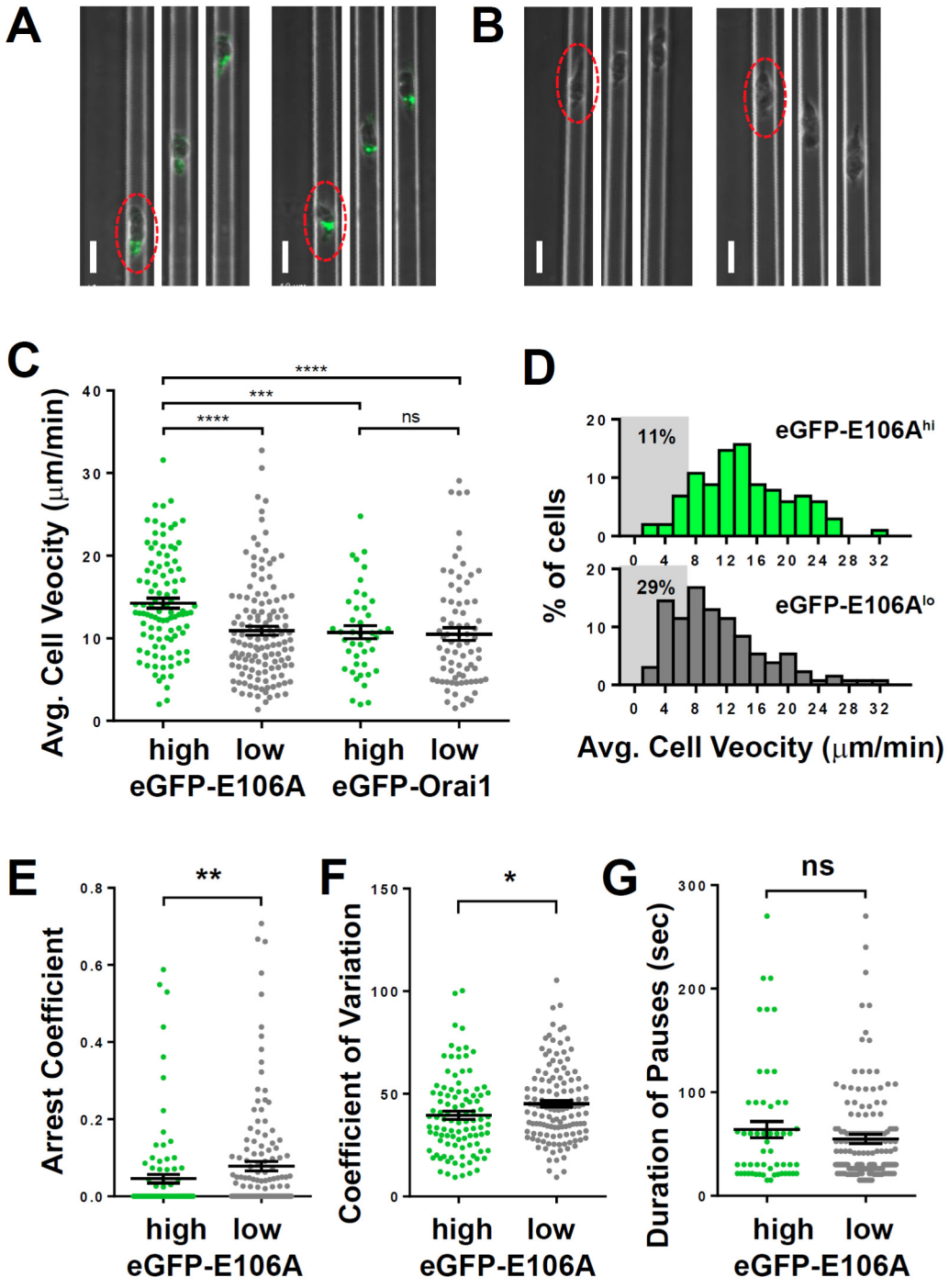

999

1000

1001 **Figure 4**

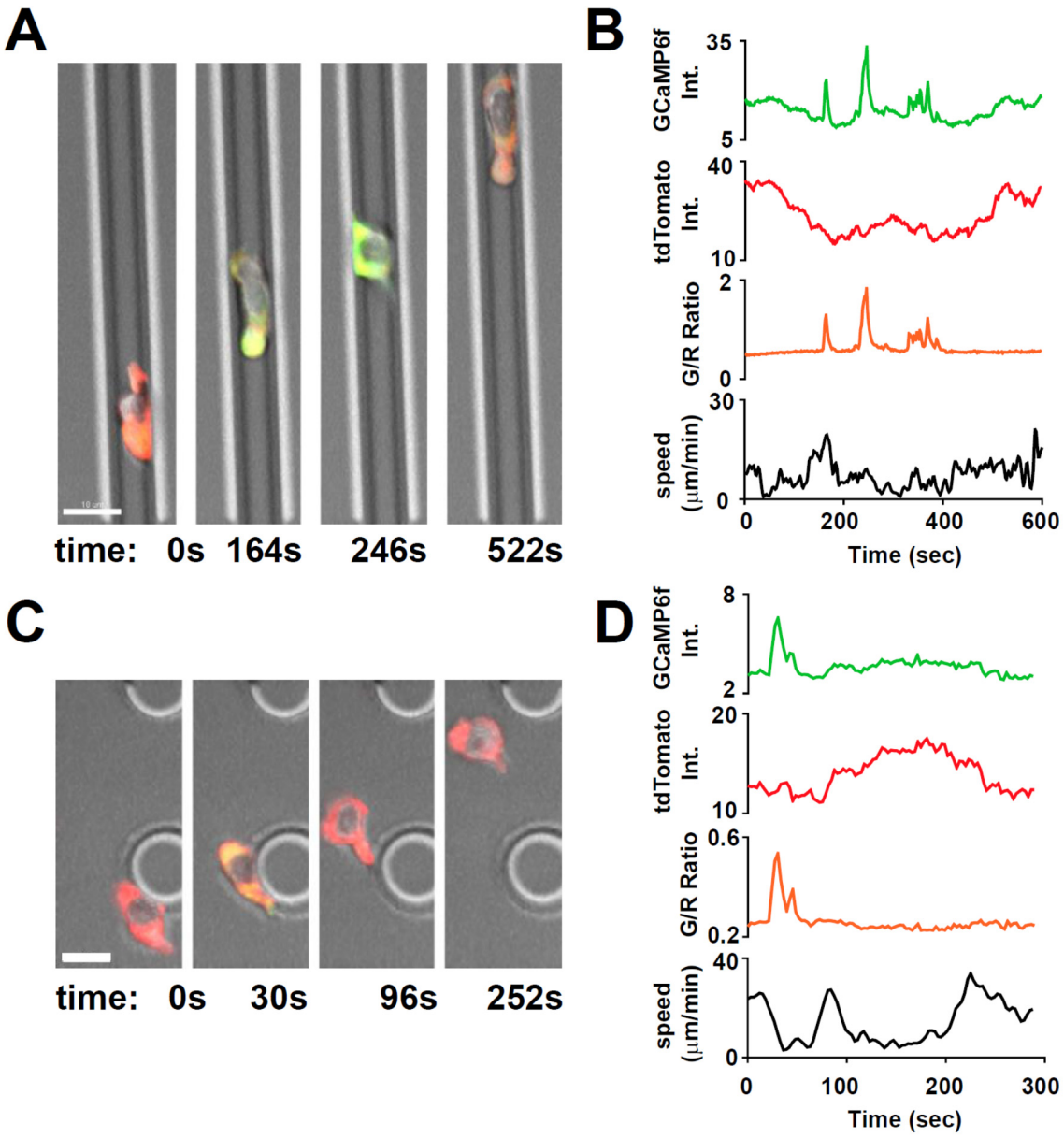

1002

1003

1004 **Figure 5**

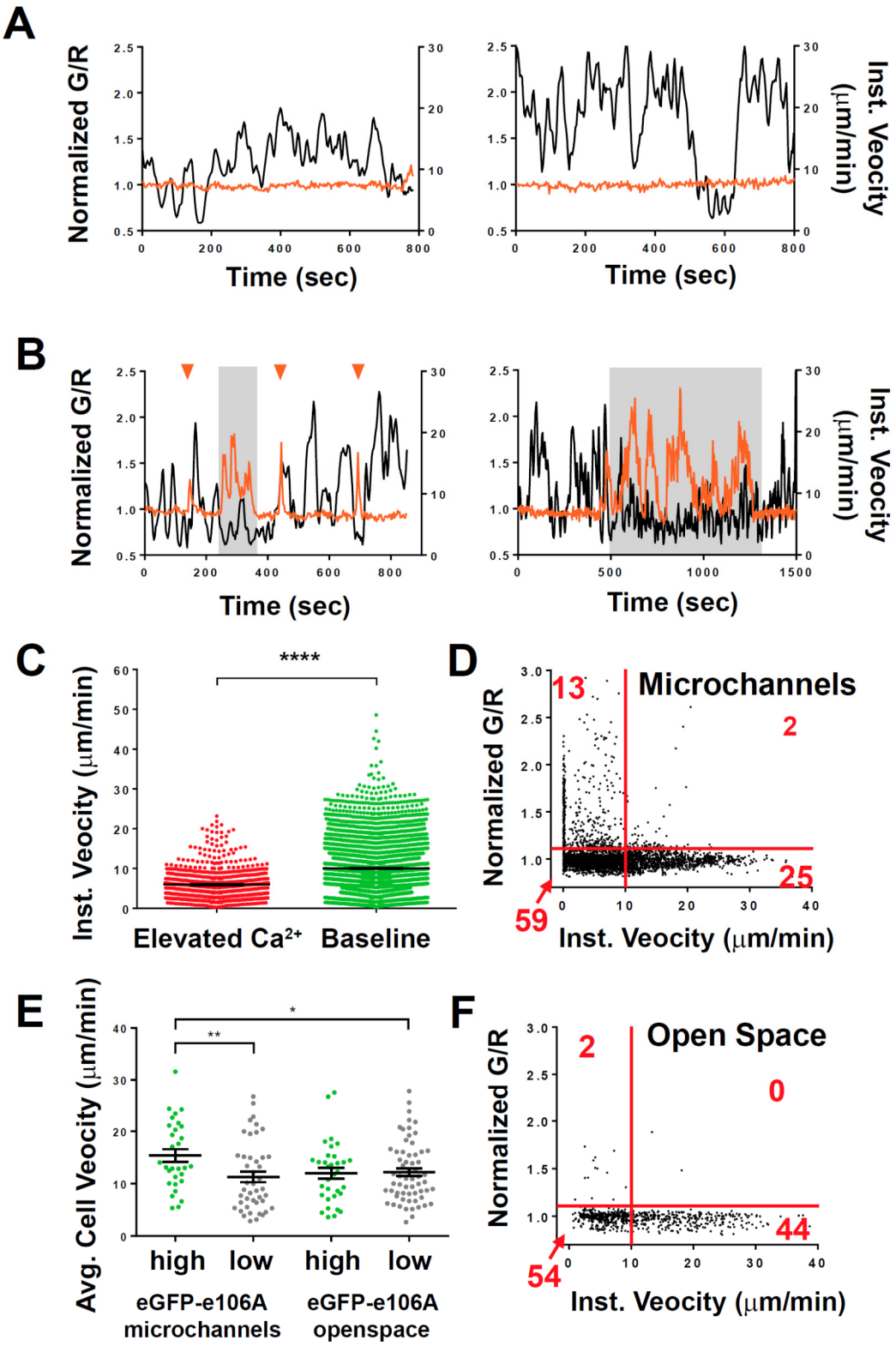

1005

1006 **Figure 5 Supplement 1**

1007

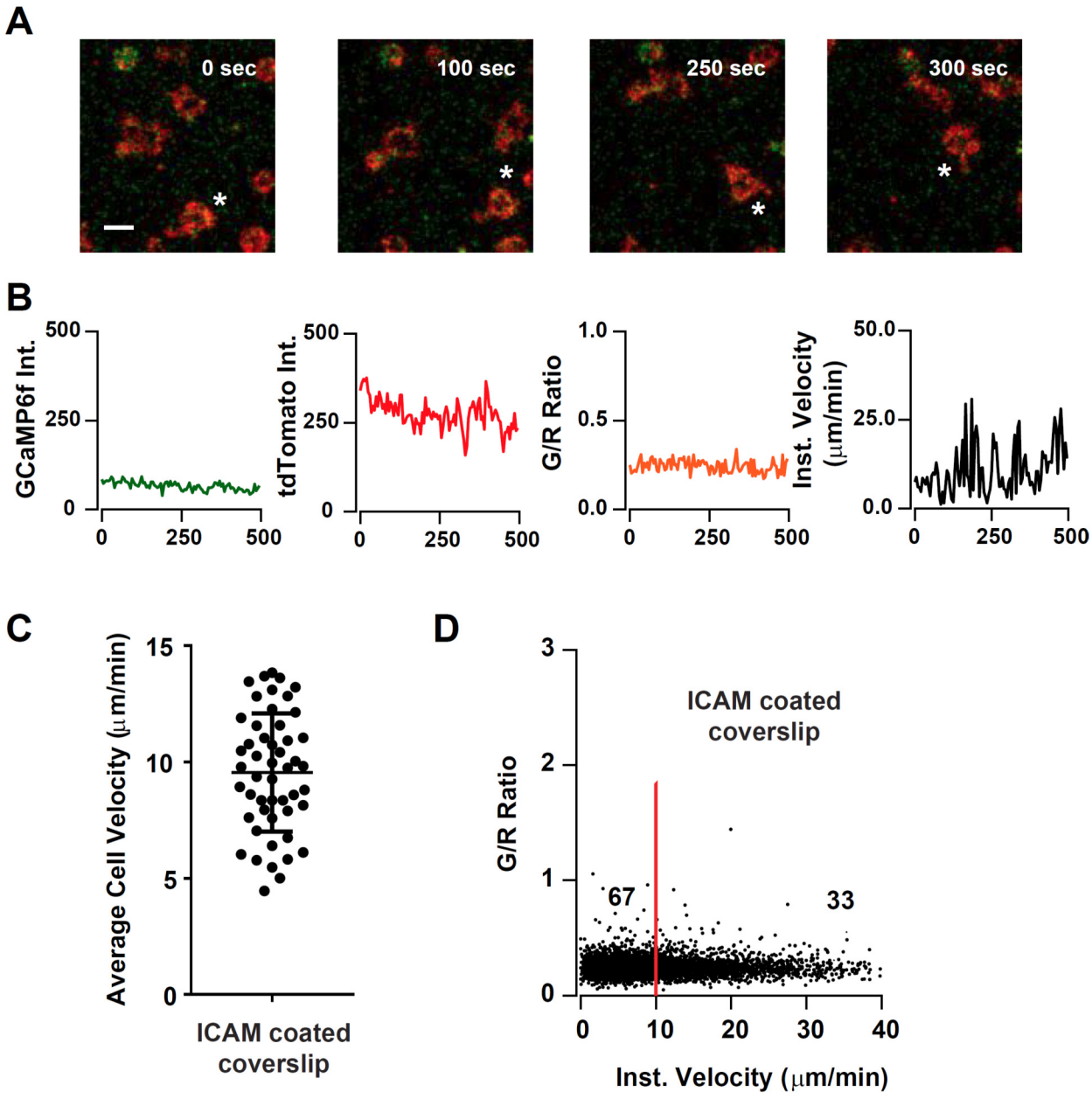

1008

1009 **Figure 6**

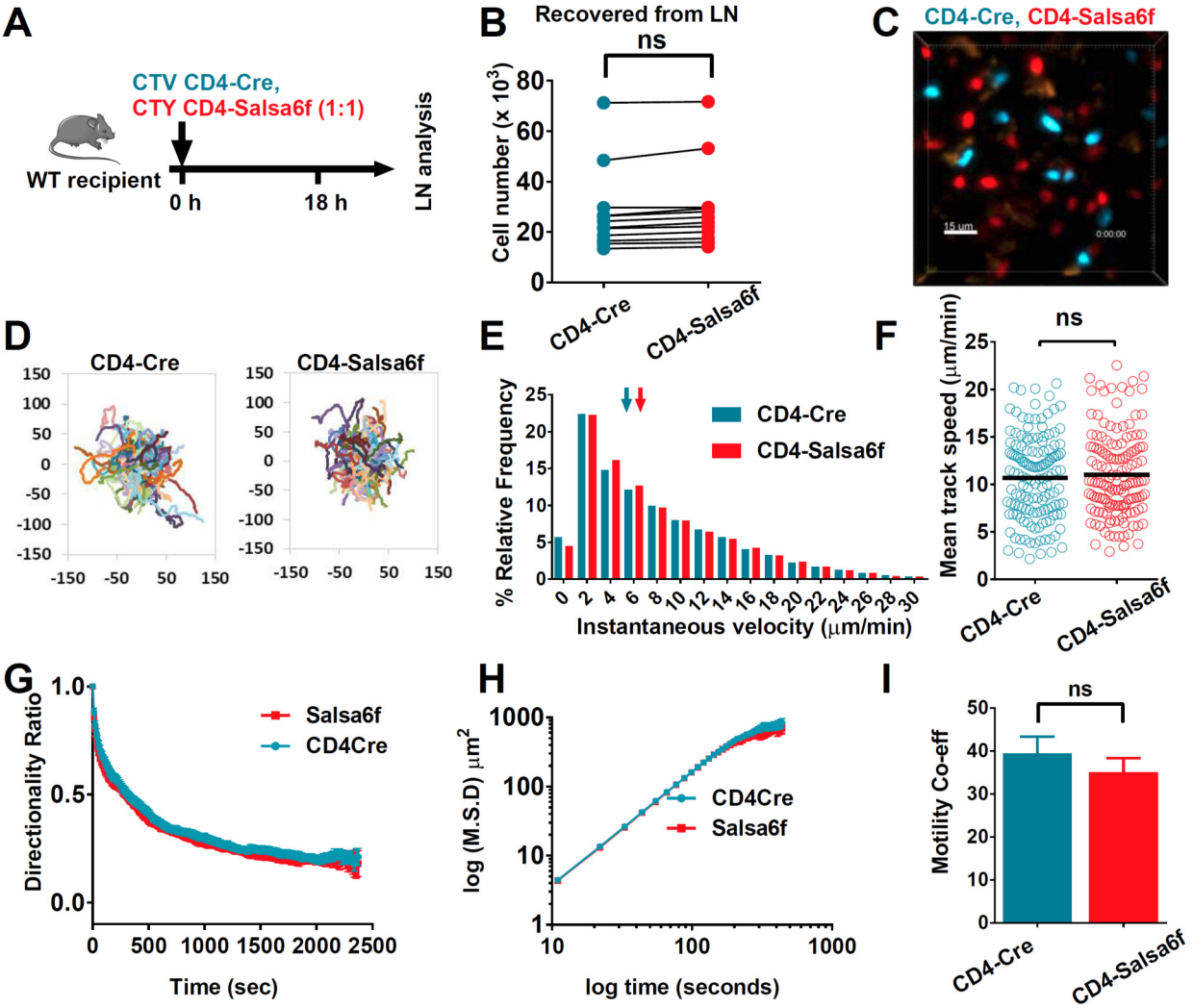

1010

1011

1012 **Figure 7**

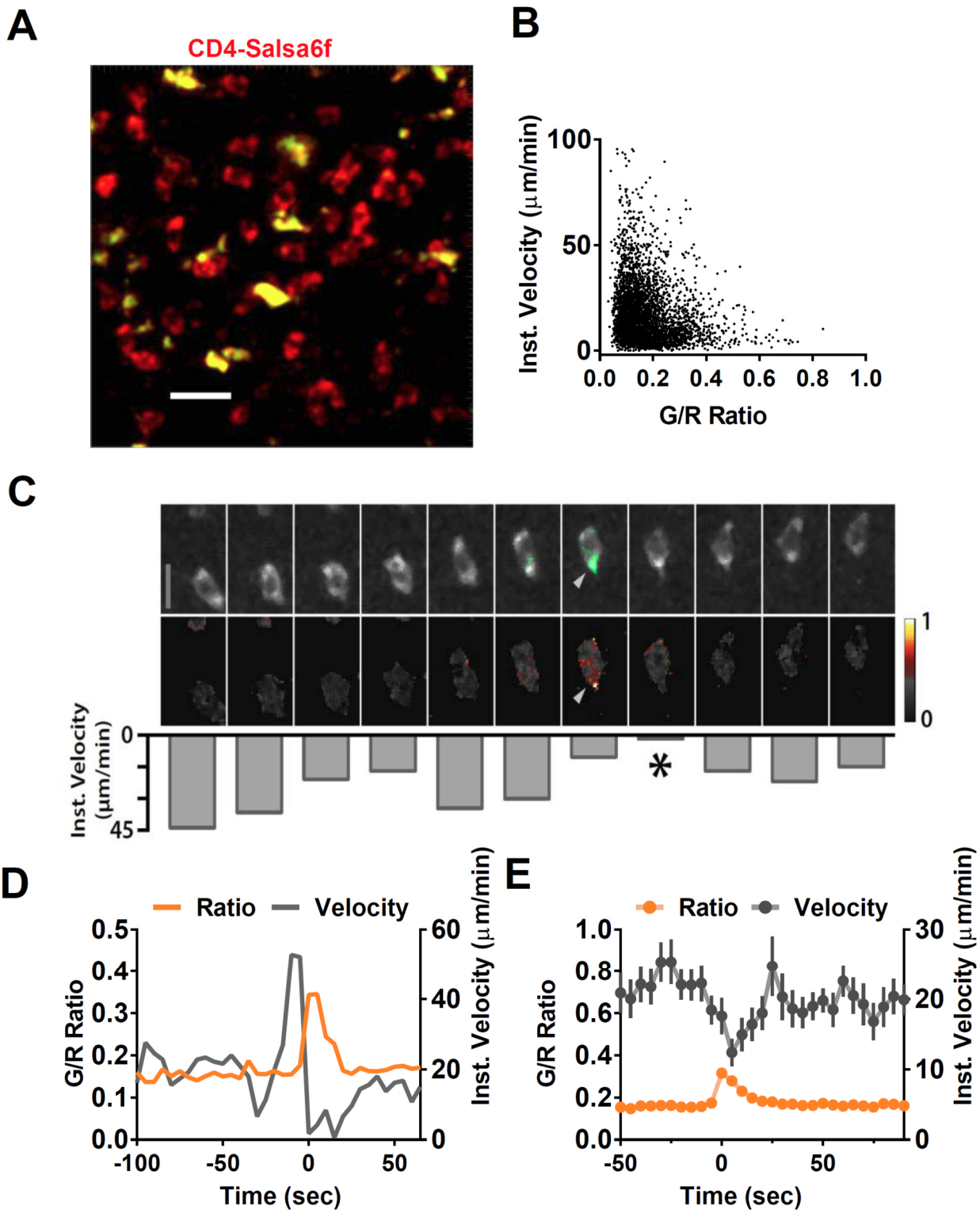

1013

1014

1015 **Figure 8**

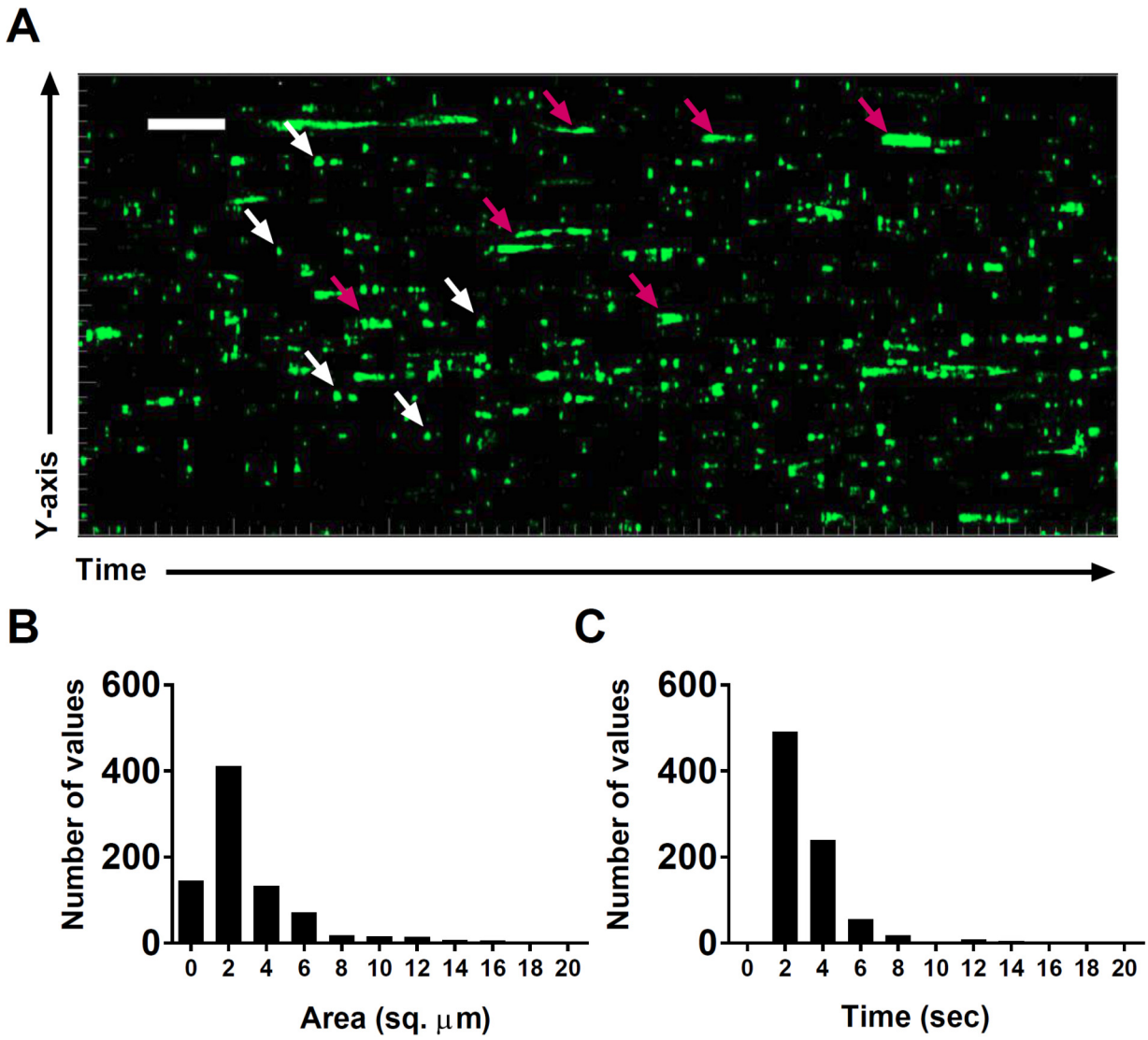

1016

1017

1018 **Figure 9**

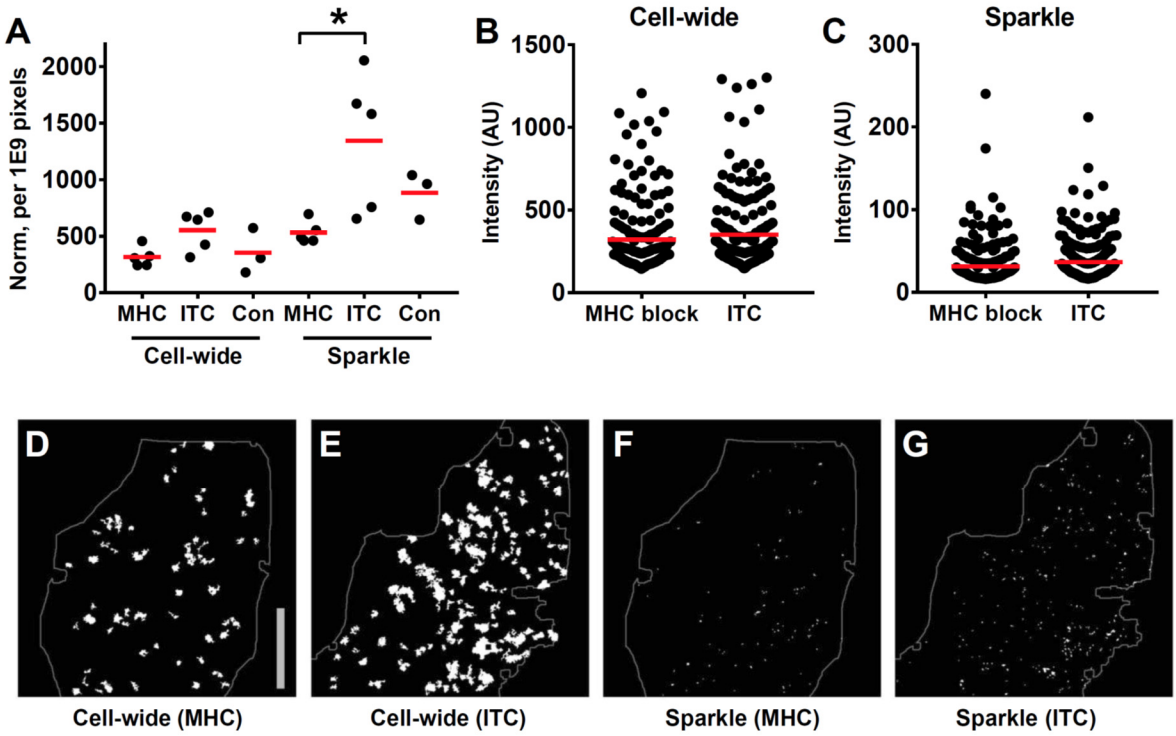

1019

1020

Video Legends

Video 1. Salsa6f-transfected human T cell in confined microchannel. Merged red (tdTomato), green (GCaMP6f), and DIC channels; scale bar = 10 μm, time shown in hr:min:sec. This video corresponds to **Figure 4A**.

Video 2 Salsa6f transfected human T cells in open microchamber, with merged red (tdTomato), green (GCaMP6f), and DIC channels, circular structures are support pillars part of the PDMS microchamber; scale bar = 10 μm, time shown in hr:min:sec. This video corresponds to **Figure 4C**.

Video 3. Motility of CD4-Salsa6f T cells in lymph node following adoptive transfer. CD4-Cre and CD4-Salsa6f$^{+/-}$ cells and their trails are shown in teal and in red, respectively. Autofluorescent bodies appear as faint stationary yellow structures. Images were acquired at ~11 second interval. Playback speed = 50 frames per second; time shown in hr:min:sec. Video corresponds to **Figure 6C**.

Video 4. Calcium signals in adoptively transferred CD4-Salsa6f T cells. Red signal from tdTomato expression in cytosol facilitates identification and tracking of cells; green GCaMP6f signal detects elevation of Ca^{2+}. Autofluorescent structures appear as stationary yellow bodies. Movie is paused at frame 323, zoomed in to emphasize two examples of Ca^{2+} transients and an autofluorescent body. Images were acquired at 5 second interval. Major tick marks at 20 μm. Playback speed = 50 frames per second, time shown in hr:min:sec. Video corresponds to **Figure 7A**.

Video 5. A brief Ca^{2+} signal filling the back of a moving adoptively transferred Salsa6f^{++} T cell. Left: composite of red tdTomato fluorescence pseudocolored grayscale

with green GCaMP6f fluorescence. Right: Corresponding Green/Red ratios, masked to red channel as in Fig. 7C. Images acquired at 1 frame every 5 sec and 0.5 microns/pixel. Playback speed = 3 frames per second. 0.5 μm/pixel. Video corresponds to **Figure 7C**.

Video 6. Calcium transients in steady state lymph nodes. CD4-Salsa6f$^{+/+}$ lymph node imaged at 0.5 second interval, processed to visualize Ca^{2+} transients (sparkles and cell-wide) in green. Red channel is turned off after beginning to facilitate viewing of Ca^{2+} transients. Autofluorescent structures appear as stationary green bodies. Playback speed = 100 frames per second. time shown in hr:min:sec. Video corresponds to **Figure 8A**